UNIVERSITY OF OKLAHOMA

GRADUATE COLLEGE

BEAM SHEAR IN MILD REINFORCED ULTRA-HIGH-PERFORMANCE CONCRETE

A THESIS

SUBMITTED TO THE GRADUATE FACULTY

In partial fulfillment of the requirements for the

Degree of

MASTER OF SCIENCE

By

JOHNATHAN MARTIN

Norman, Oklahoma

2022

BEAM SHEAR IN MILD REINFORCED ULTRA-HIGH-PERFORMANCE CONCRETE

A THESIS APPROVED FOR THE
SCHOOL OF CIVIL ENGINEERING AND ENVIRONMENTAL SCIENCE

BY THE COMMITTEE CONSITING OF

Dr. Jeffery Volz, Chair

Dr. Royce Floyd

Dr. Shreya Vemuganti

Acknowledgments

This research thesis could not have been completed without the help others, whom I would like to acknowledge. First, I would like to thank everyone in my research group for their assistance in the lab. Jackson Milner provided consistent hands-on help, Jorge Vargas provided expertise in the mixing procedure of UHPC, and Jake Choate provided his wisdom from experience in the lab. Other research students who made long days in the lab feel more manageable include Wassime Somatri, Stephen Roswurm, and Zach Tiry. A very special thank you to John Bullock, for his encouragement and camaraderie, which was even more valuable to me than his capabilities in the lab.

I want to thank my committee members, Dr. Floyd and Dr. Vemuganti, for their patience and feedback. I want to thank my committee chair and advisor, Dr. Volz, for providing this opportunity to me and doing everything he could to help me succeed.

Lastly, I want to thank my friends and family for displaying an interest in my work so I could be reminded how impressive it was to break concrete. Most importantly, I want to thank my fiancée, Melanie soon to be Martin, for being a constant driving force keeping me on track to finish.

Abstract

Ultra-high-performance concrete (UHPC) is being utilized in bridge construction primarily for deck overlays and end of girder and beam repairs of deteriorated traditional concrete elements. UHPC has been used selectively in new construction to form full sized structural members. Compared to conventional concrete, UHPC has the benefits of having a high compressive strength, being more ductile, and being self-consolidating. Because of these qualities, it can be used in very thin beams with shallower depths than a conventional concrete member could. Before it can be used on a larger scale more must be known about the failures that can occur. The current ACI Code (ACI 318-19 2019) places an upper limit on the compressive strength allowed in the shear capacity equation of 10,000 psi. UHPC can have strengths more than double this and may not behave as expected. The aim of this project was to quantify the shear capacity of UHPC beams. The testing regimen for this project included two conventional concrete beams and three UHPC beams. The mix for the conventional concrete was based on an Oklahoma Department of Transportation Class AA, having a compressive strength of approximately 9,000 psi. The UHPC followed the non-proprietary mix design develop at the University of Oklahoma, designated J3, which had a compressive strength of 17,000 psi.

The beam specimens tested were approximately a half-scale AASHTO Type B beam with some exaggerated proportions to better facilitate shear failure. All beams were of the same dimensions, having an overall depth of 16 in., an effective depth of 14.25 in., a web height of 8 in., and a web thickness of 2 in. A total beam length of 14 ft was chosen to allow for a 12-ft testing region under third-point loading. There were supports under the beam at 1 ft from each end and loading applied 5 ft from each end, giving equivalent 4-ft uniform shearing regions. All beams were fitted with a reinforcing cage having no shear reinforcement in the zones under

shear. Longitudinal reinforcement included three #6 reinforcing bars. Each member was tested at 28 days to allow for full strength development. The UHPC beams did not fail in shear. With approximately 4 in. of deflection, the beams exhibited significant flexural cracking and minor shear cracks. The maximum load for each UHPC specimen exceeded an equivalent shear capacity of over $9\sqrt{f'_c}b_w d$. From this research, it was concluded that current ACI Code (2019) design guidance is insufficiently accurate and overly conservative for UHPC members, but more research is required.

Table of Contents

List of Tables

List of Figures

Notation

A_g Cross sectional area

A_s Area of longitudinal steel

b_w Width of web

d Distance from extreme compression fiber to center of longitudinal steel

f'_c Compressive strength of concrete

N_u Axial load

V_c Shear capacity of concrete (force)

V_{test} Shear load of concrete during testing (force)

ρ_w Ratio of A_s to $b_w d$

λ Lightweight concrete factor

λ_s Size factor

$V_{Rd,c}$ Shear force resisted by concrete (from French Code)

$V_{Rd, s}$ Shear force resisted by vertical reinforcement (from French Code)

$V_{Rd, f}$ Shear force resisted by fibers (from French Code)

1 Introduction

1.1 Background and Justification

Concrete has been used in construction since before the Roman Empire. In recent decades though, this common construction material has been drastically improved upon. Ultra-high-performance concrete (UHPC) can have compressive strengths upwards of 20,000 psi, which is 5 times that of the minimum required strength for the typical bridge girder concrete, Class AA, as specified by the Oklahoma Department of Transportation (ODOT). Most of the current applications of UHPC include field casting connections for precast elements, repairs of conventional concrete, and some structural pieces. The United States Department of Transportation (DOT) maintains a database of bridges that utilize UHPC elements. One of these bridges is the Mars Hill bridge in Wapello, Iowa. This bridge was built with “three 110ft long precast concrete modified 45in deep Iowa bulb-tee beams topped with a cast-in-place concrete bridge deck. The concrete offers such considerable strength that the beams were built without any shear reinforcement” (Vance, 2012). This bridge demonstrates the incredible possibilities that can be actualized with a better understanding of the material properties of UHPC. Thinner and shallower beams can be designed when using UHPC due to its high strength and improved flowability. Currently, UHPC has limited use in large-scale projects because of costs and a lack of certainty in the design capacities.

This research studied the strength of UHPC beams in shear under a third point loading to discover if UHPC fails similarly to normal strength concrete mixes. In ACI 318-19 section R22.5.3.1 (2019), it is stated that "because of a lack of test data and practical experience with … compressive strengths greater than 10,000 psi, the Code imposes a maximum value of 100 psi on

$\sqrt{f'c}$ for use in the calculation of shear strength in concrete members." Prior UHPC research has primarily focused on either small specimens or very large, prestressed beams. There is a need for testing of large scale typical non-prestressed beam sections to develop a better understanding of beam shear in UHPC.

1.1.1 Benefits of UHPC

UHPC differs significantly from conventional concrete in terms of composition and material properties. First, UHPC does not use coarse aggregate, which is a significant portion of the volume of a conventional concrete mix. The volume of cementitious materials and fine aggregates are increased to replace the coarse aggregate. This higher volume of paste increases the workability of the concrete when placing, which may allow for tighter forms, but because of the very low water-cement ratios used also requires large dosages of high range water reducer (HRWR). The paste of UHPC is also much denser than conventional concrete, which contributes to a shorter development length for reinforcement. Also, the tighter matrix creates a more durable concrete. Another significant change is that UHPC typically includes steel fibers, granting a high post-cracking tensile strength and higher ductility. Currently, shear capacity equations are related to the tensile strength indirectly by using the compressive strength of concrete. Because of the tensile strength of UHPC is much higher than traditional concrete, UHPC specific design guidance for shear may need to directly factor in the tensile strength.

1.1.2 Concerns of UHPC

A current set of design guidelines for using UHPC does not exist in the United States. The lack of design guidance can make engineers more hesitant to branch out and use this superior concrete. In addition to the uncertainty of constructing with the new concrete, there is the cost of UHPC. Proprietary UHPC is significantly more expensive than conventional concrete.

One way to reduce the costs of UHPC would be to issue a design guidance that is not overly conservative, like the ACI Code (2019) is currently. If the capacities of UHPC are more thoroughly tested, there could be a reduction in costs through the reduction of shear reinforcement.

1.2 Objectives and Scope of Work

The objective of this study was to evaluate the shear performance of UHPC in beams, compared to conventional concrete and the ACI Code (2019). Two conventional concrete beams and three UHPC beams were tested under third point loading. A non-proprietary UHPC mix design developed at the University of Oklahoma (J3) was used to cast the UHPC beams.

1.3 Outline

This thesis consists of six chapters and an appendix. The first chapter provides an introduction into the research project. The characteristics of UHPC, the objectives of this study, and an explanation of why this study was necessary are covered in Chapter 1.

Chapter 2 is a literature review that evaluates the differences in conventional concrete and UHPC in reference to shear. This chapter also references other studies performed to develop a better understanding of UHPC.

Chapter 3 describes the process of designing the test and the fabrication of its elements. This includes the fabrication of the formwork, the reinforcement design, and the mix design for the beams.

Chapter 4 presents the strength development for each mix, the results of the tests performed, and representative photographs of the crack propagation and overall beam deformations.

Chapter 5 analyzes the results from Chapter 4 by normalizing the data, then comparing the normalized results to the shear equations from the ACI Code (2019) and an extensive database of prior reinforced concrete beam shear tests.

Chapter 6 concludes this thesis with a summary of the results and how the results were interpreted, followed by suggestions for further research.

The appendix contains photographs of the beam specimens at various breaking points. It is included to present a better visual of the entire beam breaking behavior. Some photographs of cylinders are also included to demonstrate various breaks.

2 Literature Review

The following chapter contains a review of the literature related to beam shear capacity in reinforced concrete members. The greatest amount of test data is based on conventional concrete. However, in recent years researchers have also focused on the shear behavior of new types of concrete, including fiber reinforced concrete, self-consolidating concrete, and UHPC. Shear failures are considered sudden and dangerous, two of the least desirable characteristics of a beam failure. There are ways to negate these undesirable characteristics of concrete shear, such as including stirrups or fibers. A review of the recent research on developments in shear capacity follows.

2.1 Conventional Concrete

Numerous tests have been performed on conventional concrete specimens designed to fail in shear. Figure 2-1 shows a plot of shear tests from numerous studies. For the most part, these have been standard concrete mixes testing various admixtures or aggregate replacements. The majority of the projects analyzed relied on standard shear capacity calculations and focused on verifying whether the changes to the mix design negatively impacted the shear capacity.

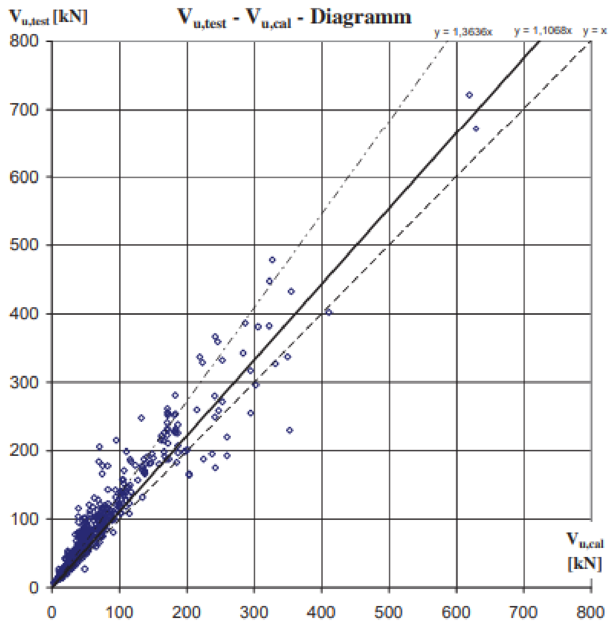

Figure 2-1: Database of shear specimens (Reineck et al., 2012)

The database for shear tests without reinforcement shows that beams designed for higher loads were more conservative in their calculation than that for lower strength beams, as shown in Figure 2-1. These specimens were on average 6,000 psi compressive strength concrete with average dimensions of 8 in. wide by 12 in. deep. Theoretically, the data would follow the lower dashed line as that line represents the test results matching the calculated capacity. However, most points are above the y = x line as indicated by the best-fit solid line.

2.1.1 Aggregate Interlock

In conventional concrete, coarse aggregate can provide extra compressive strength due to its high density. Coarse aggregates can also improve the shear capacity of a concrete specimen. When a shear crack forms it will go around the face of the coarse aggregate, leaving it embedded in one side of the crack. As the faces of the crack slide past each other, the embedded coarse aggregates provide resistance due to the increased friction. This process of aggregate interlock holds thin cracks together until the crack becomes wide enough to release suddenly. This explains the violent nature of shear failures (Drury, 2018).

In normal strength concretes, much of the shear strength comes from aggregate interlock. This can cause a large range in shear capacity because crack propagation is unpredictable. A new problem arises when using higher strength concrete, as “it appears that cracks in concrete travel right through the aggregate particles rather than around them” (Huber, 2019). With the cracking travelling through the coarse aggregate, the concrete will have a smoother failure surface, reducing the shear friction. This discovery indicates that if the failure plane is relatively smooth, there may be a reduction in shear capacity. In UHPC mixes, the only aggregate is typically a masonry sand. This sand increases the workability of UHPC at the cost of the ability for aggregate interlock to increase shear strength.

2.1.2 Dowel Action

The longitudinal reinforcement ratio (ρ) can influence the shear capacity of concrete. In some instances, the steel used as longitudinal reinforcement can provide increased stiffness in the beam. The steel can reduce the separation between the faces of cracking surfaces by providing dowel action. This effect is more influential at lower strengths. Research has shown that, “it can be concluded that the effect of ρ on the shear capacity of UHPC beams reinforced with high-strength rebars is insignificant, as in this understanding of the shear behavior of conventional RC beams” (Bahij et al., 2018).

2.2 Nonconventional Concretes

Nonconventional concretes are useful for special circumstances and can include chemical admixtures, very high compressive strengths, or physical improvements such as fibers.

2.2.1 Fiber-reinforced Concrete

As previously stated, the shear capacity is related to the ability of the concrete to prevent cracks from spreading wide enough to slip easily past each other. Fibers can be introduced into the mix to increase the tensile capacity. Research has suggested, “fibers are able to contribute to the shear strength. Beams with fibers reached higher shear ultimate loads” (Cuenca, 2009). This conclusion was reached after testing I-shaped beams with an 8” web under similar loading as the planned setup for this research.

Previously, research was performed on beams that reduced the volume of cementitious materials in the mix through aggregate optimization. This project was designed to lower the cost of concrete and make more economical mix proportions. In the testing of these eco-friendly concretes, it was demonstrated that the beams had shear strength greater than $2\sqrt{f'c}$ (Wallace, 2017). Instead of shear stirrups, these beams included synthetic fibers. These fibers were not credited with directly increasing the shear capacity of the concrete, although they were included to minimize microcracking. A crack that has already formed takes less energy to advance, so microcracks can allow easier crack propagation, making a lower load cause the beam to fail.

Other research has shown increased shear capacity when using steel fibers in high-strength concrete. “Increasing V_f in UHPC beams without shear stirrups did not only increase the shear capacity of the beams, but also changed their failure modes from shear-tension to shear compression,” where V_f was the percent of steel fibers in the beam (Bahij et al., 2017). This study correlated an increase in shear strength with an increase in percentage of steel fibers, using 1%, 1.5%, and 2%. The conclusion of this research claimed to have validated research done by Gustafsson in 1999, which showed much more efficient increases in shear capacity using fibers over stirrups.

2.2.2 Self-consolidating Concrete

Self-consolidating concrete (SCC) is a highly flowable, non-segregating concrete mix that can achieve consolidation under its own weight. Self-consolidation is an ideal property of concrete because it reduces the amount of effort needed to place the concrete into the forms. Some research has also claimed that SCC increases the tensile capacity due to the extra volume of paste.

One study claimed that “beams made of TC (traditional concrete) or SCC with an identical concrete compression strength showed identical shear behavior. No difference was found in shear strength and load-deflection behavior” (Cuenca, 2009). This implies that the increased tensile strength from the increased paste volume does not result in a corresponding increase in shear capacity. There could also be a reduction in the strength from aggregate interlock, because smoother or smaller aggregates were used for the higher flowability. However, there is a correlation between tensile strength and shear capacity. Another study stated “while tensile strength is directly linked to shear strength, concrete compressive strength (f’c) is more commonly used to compute beam shear strength. This is because tensile testing is difficult to conduct, and the relationship between the two is well understood for conventional concrete” (Drury, 2018).

From these studies, there does not seem to be a consensus in how the material properties of SCC affect the shear capacity. This would also imply that the increased ductility of UHPC should be primarily credited to the steel fibers.

2.2.3 Ultra-high-performance Concrete

Beam failure is rarely based on a single criterion because internal forces interact to cause failure. The influence of high steel density for longitudinal reinforcement changing the shear capacity is an example of this interaction. Because of these interactions and the relative newness of UHPC, analyzing the other properties is pertinent. Research has indicated that the bonding strength of UHPC is much higher than predicted by the standard ACI and AASHTO methods (John et al., 2011). By testing development length in flexure, the study was able to show that the properties of the UHPC, not directly related to strength, were able to provide benefits typically associated with strength. Based on this study, it is likely that the increased tensile capacity of UHPC, which allows for the shorter development length, will increase the shear capacity beyond what is predicted by the ACI Code (2019). This also connects to the ability of the concrete to resist a strand being pulled out of either face across a crack.

Developing a sufficient way to accurately predict the tensile capacity of UHPC is still an on-going process. Research performed at the University of Oklahoma has attempted to solve this in a few ways. A cylindrical section with a tapered center was developed to test different fiber contents (Lepissier, 2020). This specimen was a modified dog bone designed to reduce stress concentrations and provide a better way to tension the member. Another testing regimen was developed using rectangular prisms to validate the research performed by Lepissier. The testing setup for this project was based on a test design developed for the Federal Highway Administration (Graybeal and Baby, 2019). This research concluded the same as Lepissier, that the range of 2%-4% fibers showed improvement in tensile capacity (Campos, 2021). Both sets of test specimens demonstrated post-cracking strength. In testing of conventional concretes, a failure of a prismatic section in tension is typically a single sudden crack. The findings from these projects indicate that the shear in UHPC may be significantly different from conventional concretes.

Research conducted at the University of Washington using the same non-proprietary UHPC mix sought to quantify the shear capacity of UHPC with steel fibers (Voytko et al., 2022). This study used a novel testing apparatus designed to induce bilateral 2D principal stresses in a panel specimen. The testing regimen for this project included testing 5 panels with different sources for the material and one varying fiber content. The results of these test showed that the increasing fiber content had diminishing returns, with the 1% fibers having roughly 75% of the shear strength as the 2% fiber specimens. The shear capacity of the panels was determined to be approximately 1,400 psi for concrete with a strength of 18,000 psi. This is significantly higher than the value $2\sqrt{f_c{}'}$ that would be used in beam shear, which would be 268 psi.

3 Test Specimen Design, Layout, and Fabrication

3.1 Introduction

This chapter will present the development, fabrication, and testing of the beam specimens. There were two Class AA and three UHPC beams created using the same formwork and reinforcing cages. The beams, cages, and testing setup were designed to encourage shear failure.

3.2 Test Setup

The goal of this project was to test the shear capacity of UHPC beams. To best accomplish this, a beam specimen was designed to be tested under third point loading. The third point loading test method is designed to create zones of constant and equal shear near each support and a constant maximum moment in the center region of the beam. The layout for the test setup is shown in Figure 3-1. The beam specimens had an overall length of 14 ft and a simply-supported span length of 12 ft, with the loads applied at 4 ft from the supports. Theoretically, the way this test is arranged would cause the two outer regions of the specimen to fail in shear at the same load. For practical purposes, the beam will typically fail on one side first due to slight variations in strength, rather than a simultaneous failure of both shear regions.

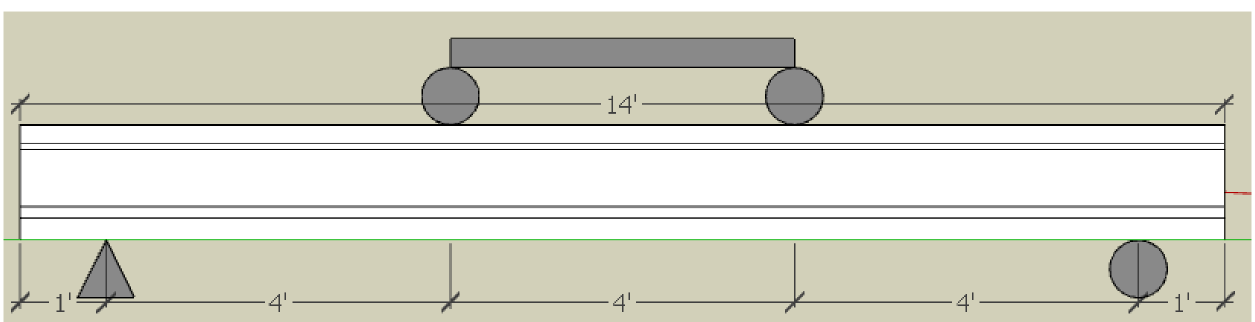

Figure 3-1: Beam test setup with third point loading

Standard Oklahoma Department of Transportation (ODOT) girder cross sections served as a basis for the beam cross section. The testing setup dictated a range for the required depth of the specimen, which was then used to scale the other dimensions downward. The spreader bar used in the testing measured 4 ft in length. The spreader bar applied the two point loads from a single hydraulic jack, which set the length of the other two regions to be 4 ft as well. The shear span to depth ratio, a/d, was then considered to avoid deep beam effects. To avoid being classified as a deep beam, the distance between loading points (a) over the depth (d) of the beam must be greater than 2 according to ACI 318-19. However, to ensure a representative beam shear type of failure, the a/d ratio should be equal to or greater than 3. With a 48 in. horizontal spacing between the support and the applied load, a 14.25 in. effective depth provides a sufficiently shallow beam to avoid deep beam effects and ensure a beam shear failure mode. The cross section of the beam is shown in Figure 3-2. The section is roughly one-half scale of a full-sized 30-ft Type B girder designed for prestressed concrete from ODOT. The web portion was designed to be slightly taller, making the web one-half of the overall beam depth, which reduced the height of the slanted regions. The web was also made thinner to reduce the shear capacity without changing the flexural capacity.

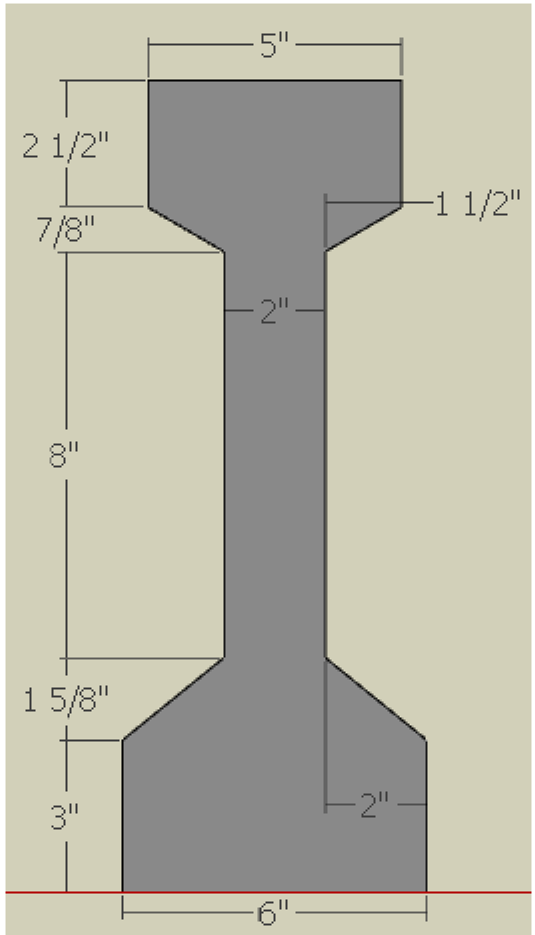

Figure 3-2: Beam dimensions

For the physical test setup, the beams were loaded into a steel frame on top of a steel beam that had been leveled. The beams were marked at distances of 1, 5, 7, 9, and 13 ft from one end. The 7 ft mark on the beam was used to center the specimen underneath the 100 kip load cell. Next, the supports were inserted under the 1 and 13 ft marks, with a pinned support on the north end and a roller support on the south end. Lastly, the loading points were inserted above the 5 and 9 ft marks. Supports and load points were steel rollers on steel bearing plates. For the first 3 beams, these rollers were arranged with 4.5-in.-diameter rollers on the bottom and 6.5-in.-diameter rollers on the top. This arrangement was necessary due to the height of the lifting hooks for the first specimen. It was kept this way until after the first UHPC beam specimen test, which revealed it was necessary to swap the rollers to have enough clearance to allow for the deflections that the UHPC beams were achieving. On both sides of the beam, at the 7 ft mark, a metal bracket was glued on at about mid height. These angles were attached via a hook to a wire potentiometer (pot). The two wire pots were used to measure the average midspan deflection. The deflection of the beam was also taken manually based on a laser level attached to the spreader bar directed at the ruler on the column to verify accuracy. As the beam deflections became more extreme, the manual measurements ceased to agree with the true deflection. The spreader bar remained straight throughout the test, therefore not measuring any deflection between the loading points. The complete testing setup is shown in Figure 3-3, where the south end is the left side of the photograph.

Figure 3-3: Testing setup

3.3 Specimen Fabrication

The beams were fabricated using a single set of reusable wooden forms. Each beam also used the exact same reinforcing layout.

3.3.1 Formwork

The formwork was constructed using plywood, 2x4's, Ellis board, screws, and wood glue. Ellis board is a high-quality plywood with a smooth waterproof finish. To construct the formwork, 28 rib pieces were cut from plywood to support slender longitudinal sections of Ellis board. With the beam measuring 14 ft in length, it was necessary to cut a 6 ft and 8 ft section of Ellis board for each segment of the face, which were placed end to end. The slender pieces were staggered from top to bottom to avoid any weak spots in the formwork caused by a straight vertical seam. All of the face pieces were screwed into each rib and wood glue was used to seal between each piece. To add stiffness to the walls, two 2x4's were installed along the length of each side. Figure 3-4 shows the rib pieces preset to receive the stiffening 2x4's and the face pieces. Figure 3-5 shows the two long walls of the form finished and at the approximate spacing for casting. In addition, two face plates were cut from Ellis board for the ends.

Figure 3-4: Rib pieces in place for face pieces

Figure 3-5: Finished sides of formwork

After finishing the two long walls, a casting bed of plywood was assembled. This casting bed included an additional 2x4 fixed at the appropriate outer distance behind each wall. The boards prevented the long sides from sliding apart, as well as maintaining a consistent layout of the formwork. The casting bed was leveled directly on the ground. This setup is shown in Figure 3-6.

Figure 3-6: Finished formwork

3.3.2 Reinforcement

The reinforcement for the beam specimens was designed to ensure a shear failure prior to any flexural failure, either yielding of the longitudinal steel or compression failure of the top flange. No stirrups were placed within the shear test regions of the specimens. The longitudinal reinforcement was designed to provide approximately three times the flexural capacity compared to the anticipated shear failure load. This was calculated using strain compatibility for a reinforced concrete beam. A compressive strength of 18,000 psi was assumed and the contribution of the fibers to flexural capacity were not considered.

The reinforcing cage was assembled using standard Grade 60 rebar and wire ties. The steel cages consisted of 3 #6 longitudinal bars in the bottom bell and 1 #3 longitudinal bar on the top to help secure the stirrups. Stirrups and cross ties were fabricated from #3 bar as well. The cross ties that were used to confine the longitudinal reinforcement were placed at 1 ft intervals and started at 6 in. from either end. Figure 3-7 shows the layout of the stirrups, represented by the vertical lines, relative to the loading and support points. Because this beam was designed to test the shear capacity of the concrete, no shear reinforcement was placed in the two test regions loaded with uniform shear.

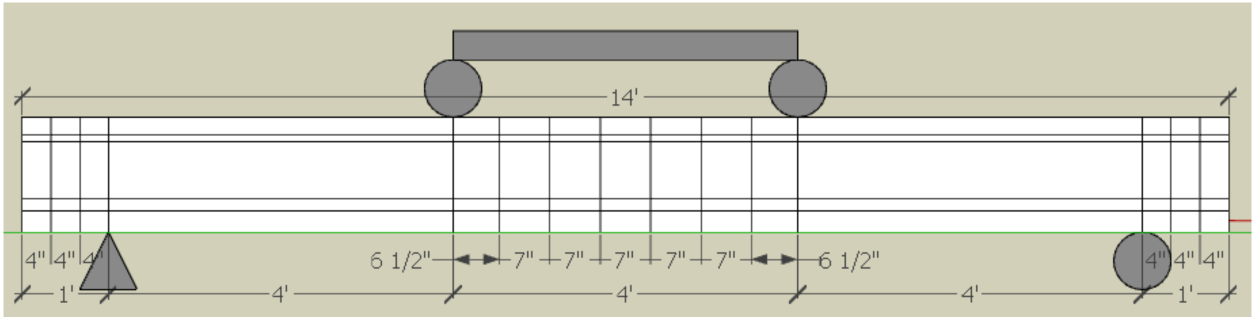

Figure 3-7: Stirrup spacing

Due to the thin web and configuration of the longitudinal reinforcement, a standard C-shaped stirrup would not have fit appropriately. To rectify this, the C-shaped stirrups were bent into a question mark shape, moving the web portion more toward the center. Figure 3-8 shows the benefits of this slight modification. Figure 3-9 shows a completed cage, where the top and bottom bars were tied using the modified C-shaped stirrups. To minimize the width of the cage, the stirrups and crossties were skewed to fit tightly. The cages were also fitted with 1 in. chairs to maintain the necessary cover on the bottom. Figure 3-10, Figure 3-11, and Figure 3-12 show how the cage fits within the formwork.

Figure 3-8: Standard stirrup vs. modified

Figure 3-9: Completed reinforcing cage

Figure 3-10: Horizontal placement of cage

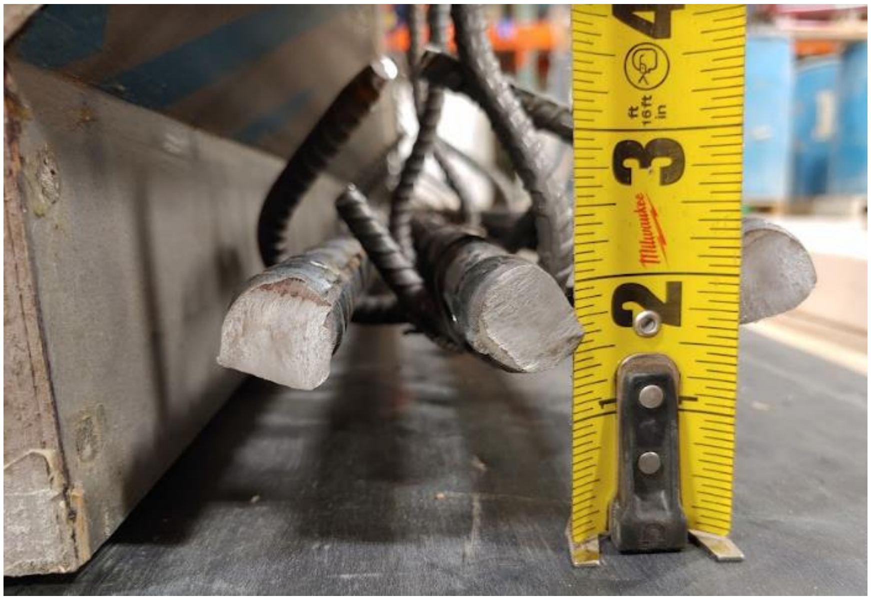

Figure 3-11: Vertical placement of cage

Figure 3-12: Cage between both walls of formwork

After the cages were placed between both formwork side walls, clamps were placed to set the appropriate top width. The cage was zip-tied to these clamps to ensure the cage remained centered. Appropriate cover was provided on all members according to ACI 318-19 Table 20.5.1.3.3 (2019). It should be noted that the minimum required straight extension of the stirrup hooks given by ACI 318-19 Table 25.3.2 (2019) was not possible with the designed cross section. The hooks were fabricated to be as long as possible without interfering with concrete placement.

3.3.3 Casting Procedure

The preparations for casting included coating the forms in form release and stretching two layers of plastic across the bottom of the beam area to prevent damage to the casting bed. Also, the bottom edges of the forms were sealed to the plastic using silicone to prevent the concrete from leaking under the form. The form release was given at least 24 hours to dry before applying the silicone. The silicone was then allowed to dry for 24 hours before placing concrete in the forms. Due to the dimensions of the beam, the cage had to be inserted before the second side form was put in place. In addition to the beam forms, cylinders were made for compressive strength testing. For the Class AA mix, 4 in. x 8 in. cylinder molds were used. For the UHPC, 3 in. x 6 in. cylinder molds were used. Every batch included at least 18 cylinders to have 3 to test on each day. The cylinders were made for 1, 3, 7, 14, and 28 days, as well as a set for test day.

During casting, 5 in. wood blocks were placed between the top faces of the forms and clamped tight to ensure a proper top width. Once the concrete had filled through the web, these blocks were removed as the pressure from the concrete was enough to keep the clamps from falling. After approximately 3 hours, the concrete was stiff enough to cover the top surface in wet burlap. Both the cylinders and the beams were allowed to cure in the molds for at least 24 hours. After being demolded, the specimens and cylinders were wrapped in wet burlap and covered in plastic. The burlap was kept moist for 7 days after casting, at which point the specimens were left at ambient temperature and humidity.

3.4 Mix Design

3.4.1 Class AA Concrete

For the conventional concrete, an ODOT Class AA concrete mix was used. The Class AA mix is ODOT's standard bridge girder mix for non-prestressed concrete. The mix was intended to be self-consolidating. A higher proportion of sand was added as well as fly ash to increase the amount of paste present in the mix. Due to the tightness of the form and cage, the mix was batched using limestone aggregate with a maximum aggregate size of 5/8 in.

A large high shear horizonal axis paddle mixer capable of mixing over 15 c.f. of concrete was used for all batches in this study. The mixing procedure was to first add the coarse and fine aggregates while the mixer was running. After allowing the aggregate to become homogenous, half of the batch water with half of the HRWR was added to the mixer. The HRWR used in all mixes for this project was Glenium 7920. This was allowed to mix for 3 minutes before the cement and fly ash were added. After the cementitious material had mixed for 3 minutes, the remainder of the water was added with the other half of the HRWR. An additional dosage of HRWR was prepared in case it was needed to increase the flowability of the mix. During mixing, the concrete was not allowed to rest. When the mix was seen to be homogenous, the concrete was released into a hopper that was attached to the overhead crane. The hopper was then used to transport the concrete to the form for filling. While the concrete was being placed into the form, the form was tapped with rubber mallets and vibrated with an internal vibrator. Meanwhile, some of the mix was released into a wagon to be used to perform a slump-flow test and fill the cylinder molds.

3.4.1.1 Class AA Concrete - Beam 1

The mix design for the first beam specimen is presented in Table 3-1. The measured slump flow for this batch was 26 in. This mix had a small amount of bleeding but did not segregate. The final dosage of HRWR was 12.25 oz/cwt.

Table 3-1: Mix for beam RC-B1

Batch Quantities for 10.8 ft^3 of Class AA	
Cement	195.6 lbs.
Fly Ash	49.0 lbs.
Water	90.8 lbs.
Coarse Aggregate	740.2 lbs.
Fine Aggregate	549.2 lbs.
Air Entrainer	10.8 mL
HRWR	885 mL

3.4.1.2 Class AA Concrete – Beam 2

The mix design for the second beam is presented in Table 3-2. The measured slump flow for this batch was 21 in. This mix was visibly less fluid, but the concrete still achieved proper consolidation with the associated vibration. The final dosage of HRWR was 12.25 oz/cwt. On this batch, a pressure method air content test was performed, which revealed an air content of 4%.

Table 3-2: Mix for beam RC-B2

Batch Quantities for 9.60 ft^3 of Class AA	
Cement	173.8 lbs.
Fly Ash	43.4 lbs.
Water	80.6 lbs.
Coarse Aggregate	649.6 lbs.
Fine Aggregate	447.2 lbs.
Air Entrainer	9.6 mL
HRWR	869 mL

3.4.2 Ultra-high-performance Concrete

The UHPC mix design was based on previous research at the University of Oklahoma (Looney et al., 2019). This UHPC mix, designated J3, achieves a design strength of 18.0 ksi and includes 2% steel fibers by volume. The fibers included in the mixes were straight copper coated 0.2 mm x 13 mm steel fibers from Hiper Fiber. The design flow is 10 in. At this flow the fibers are still suspended in the concrete until cured. As part of each UHPC mix, 3 in. x 6 in. cylinder molds were used to fabricate compressive strength specimens to verify the strength of the mix at various ages, including test day for the associated beam specimen. Upon grinding of the cylinders before breaking, the density of fibers on the top face and bottom face were noted. The fibers were slightly denser on the bottom face than the top face, but a proper distribution of fibers was still achieved.

The mixing process for the UHPC is more complex than for typical concrete. The same mixer was used for the UHPC as the Class AA concrete. All the dry materials were added to the running mixer at the beginning, except the steel fibers. The dry materials were then mixed for 10 minutes. Just before the end of the 10 minutes, half of the HRWR was added to the batch water. At the end of the 10 minutes, all the batch water was added over the course of 2 minutes, with care to spread it evenly. The materials were then allowed to mix for 3 minutes. The other half of the HRWR was then added over the course of 1 minute. At this point, the mixer contained all the materials except for the steel fibers. The materials were then allowed to mix until the concrete began to stick to itself. During this mixing, the temperature of the mix was monitored for an increase in heat. If such an increase in heat occurred, more HRWR was added. After the concrete became a flowable dough-like consistency, the fibers were added in a way that avoided large clumps. The fibers were then allowed 3 minutes to mix before the batch was finally released into the hopper. The total mixing time varied but was typically around 25 minutes.

3.4.2.1 UHPC - Beam 3

The mix design for the first UHPC beam is presented in Table 3-3. The flow for this mix was 10 in. Initially, the HRWR was batched for 21 oz/cwt, but it was necessary to add 40% more to obtain the right consistency of the mix. This mix took about 8 more minutes of mixing than the other two that had higher initial doses of HRWR.

Table 3-3: Mix for beam UHPC-B3

Batch Quantities for	7.2 ft^3 of UHPC
Cement	314.6 lbs.
Silica Fume	52.4 lbs.
GGBFS	157.2 lbs.
Masonry Sand	524.2 lbs.
Steel Fibers	70.6 lbs.
Water	104.8 lbs.
HRWR	4458 mL

3.4.2.2 UHPC - Beam 4

The mix design for the second UHPC beam is presented in Table 3-4. The flow for this mix was 10 in. Initially, the HRWR was batched for 26 oz/cwt, but it was necessary to add 20% more to obtain the right consistency of the mix.

Table 3-4: Mix for beam UHPC-B4

Batch Quantities for	6.5 ft^3 of UHPC
Cement	284.0 lbs.
Silica Fume	47.4 lbs.
GGBFS	142.0 lbs.
Masonry Sand	473.4 lbs.
Steel Fibers	63.6 lbs.
Water	94.6 lbs.
HRWR	4367 mL

3.4.2.3 UHPC - Beam 5

The mix design for the third UHPC beam is presented in Table 3-5. The flow for this mix was 10.5 in. Initially, the HRWR was batched for 26 oz/cwt, but it was necessary to add 20% more to obtain the right consistency of the mix. This mix was larger than the other two because a different research project was using some of the material.

Table 3-5: Mix for beam UHPC-B5

Batch Quantities for 9.0 ft^3 of UHPC	
Cement	393.2 lbs.
Silica Fume	65.6 lbs.
GGBFS	196.6 lbs.
Masonry Sand	655.4 lbs.
Steel Fibers	88.2 lbs.
Water	131.0 lbs.
HRWR	6047 mL

4 Test Results

4.1 Introduction

This chapter will present the test results from the compressive strength tests and the tests of the beam specimens under third point loading. The compressive strength (f’c) was measured in general accordance with ASTM C39 (2021). The load and deflection readings were recorded 10 times every second for the duration of the test on all beam specimens. All beams were tested 28 days after casting.

4.2 Class AA Concrete

Two Class AA concrete beams were tested as a proof of concept, to show the beams failed at the expected shear load. A graphical representation of the tests performed are presented in the following figures. Figure 4-1 shows the compressive strengths of the Class AA concretes used in the beam specimens. Figure 4-2 shows a load-deflection plot for both beam specimens. The periodic decreases in load coincided with pauses in the test to mark the cracks in the beams and take photos. Together these graphs can provide insight into how the specimens responded to the loading.

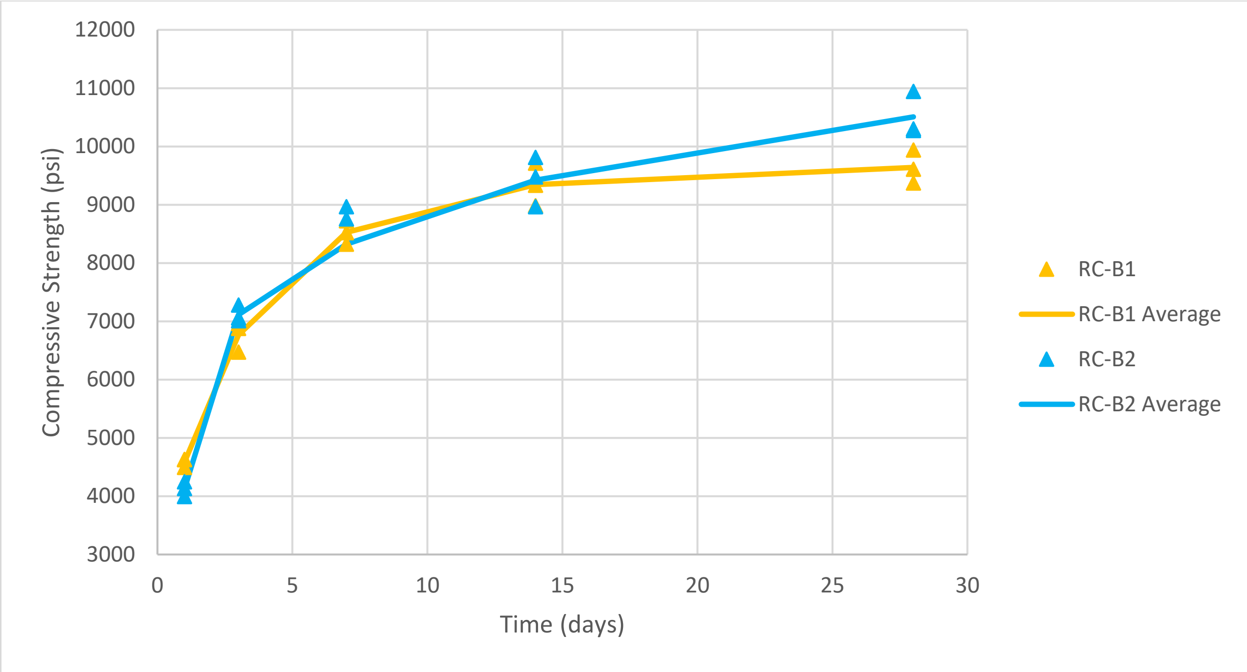

Figure 4-1 : Compressive strengths of Class AA concrete

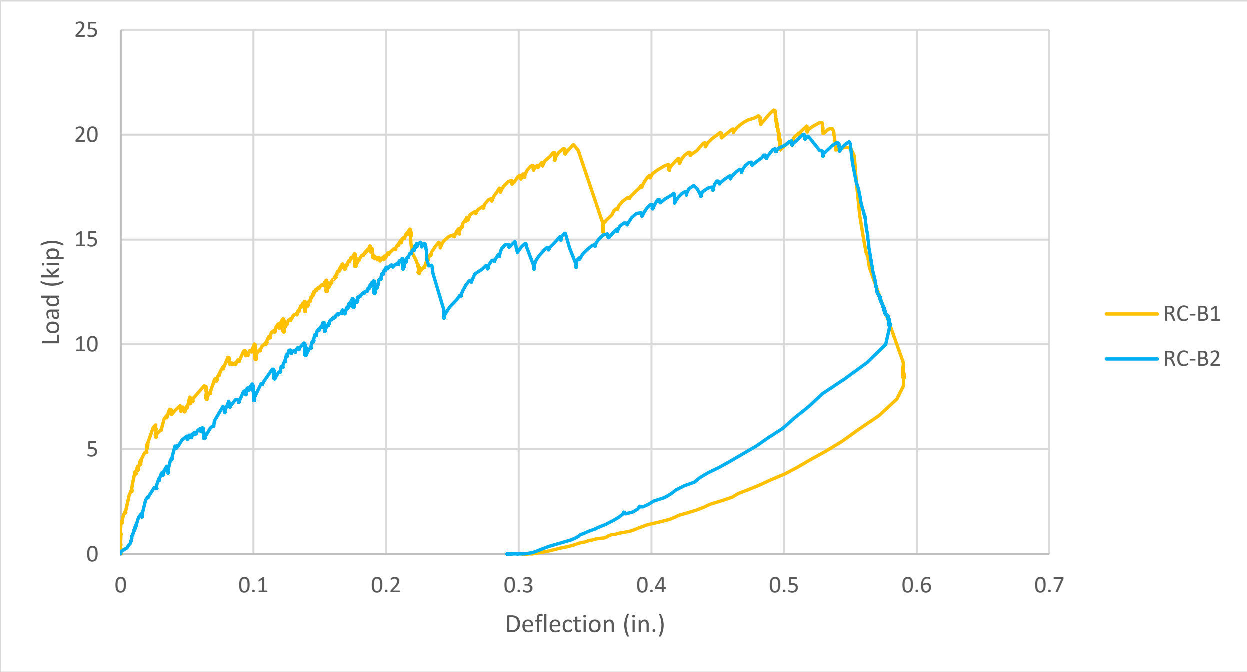

Figure 4-2: Load vs deflection for Class AA beams

A summary of the results of the Class AA concrete specimens is shown in Table 4-1. The load at shear failure was read directly from the load cell, meaning the shear force in the beam was half of the load at failure. Similarly, the max load was the total load applied at the center of the spreader bar. The testing was stopped when the beams reached ultimate failure, which was buckling of the top flange in both cases.

Table 4-1: Max results from Class AA concrete specimens

	RC-B1	RC-B2
28-day f'c (psi)	9,640	10,510
Load at shear failure (kip)	15.50	14.89
Max load (kip)	21.97	20.02
Max deflection (in.)	0.59	0.58

The Class AA beams were loaded at 2 kip intervals until cracks became visible. Both RC-B1 and RC-B2 began developing flexural cracks just before reaching 10 kips total load as shown in Figure 4-3.

(a)

(b)

Figure 4-3: Flexural cracks begin in RC-B1 (a) and RC-B2 (b)

After the cracks had appeared, the loading increment was decreased to 1 kip. All cracks were marked after each load interval. Shear cracks began to form in the beams at around 13 kips total load. A large shear crack occurred soon after in both beams. In RC-B1, this occurred at 15.50 kips total load and coincided with an audible popping sound, while in RC-B2, this occurred at 14.89 kips and also coincided with an audible popping sound. These cracks are evidenced by the first sudden drop in load on Figure 4-2. The cracks are shown in Figure 4-4.

(a)

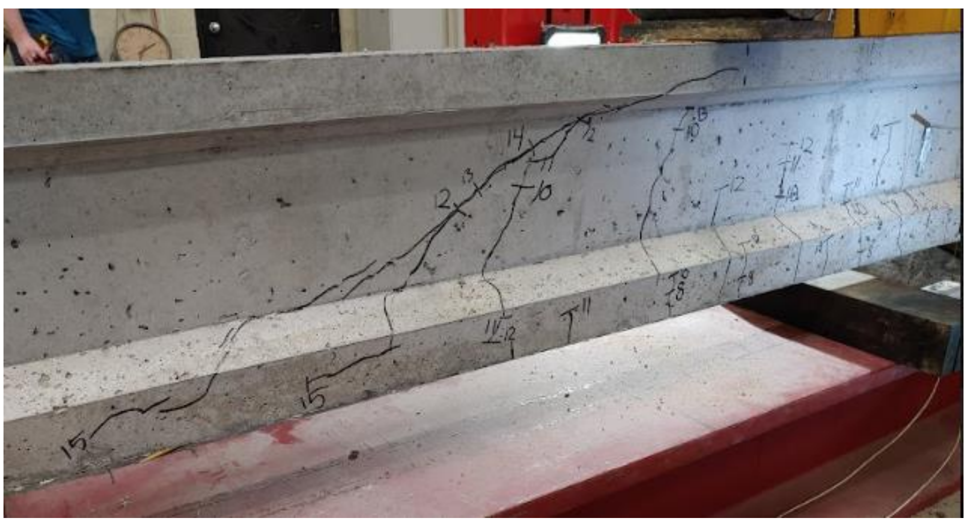

(b)

Figure 4-4: Shear crack in RC-B1 (a) and in RC-B2 (b)

After the initial shear crack occurred, the beams were loaded until the top flange eventually buckled at the maximum total load, at which point the beam was unloaded. The load and deflection readings were taken until after the beam was fully unloaded. The ultimate failure of each beam is shown in Figure 4-5.

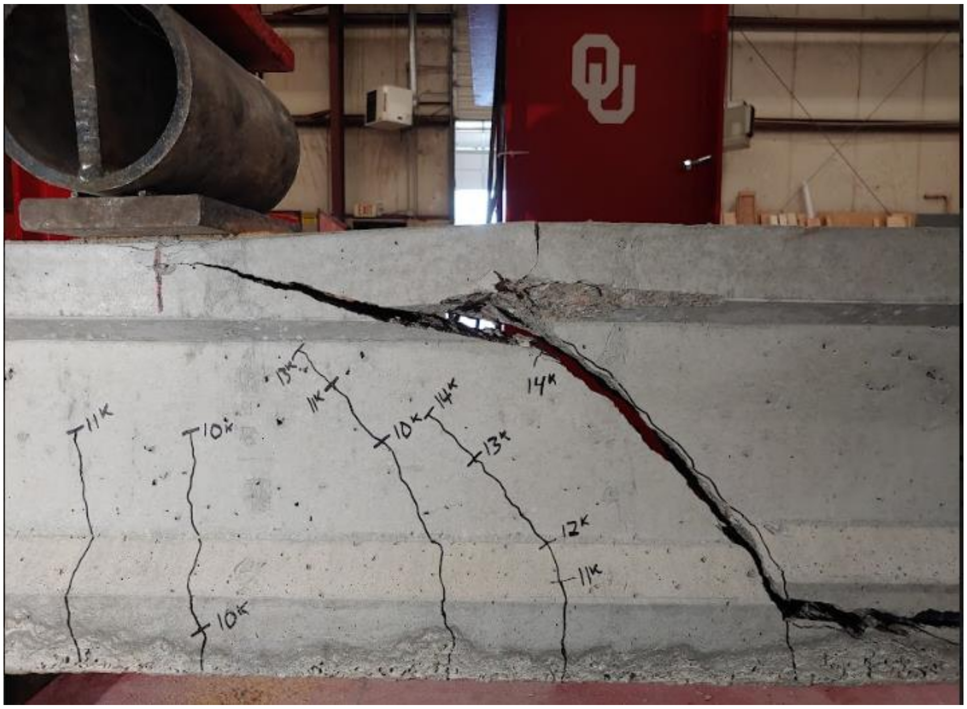

(a)

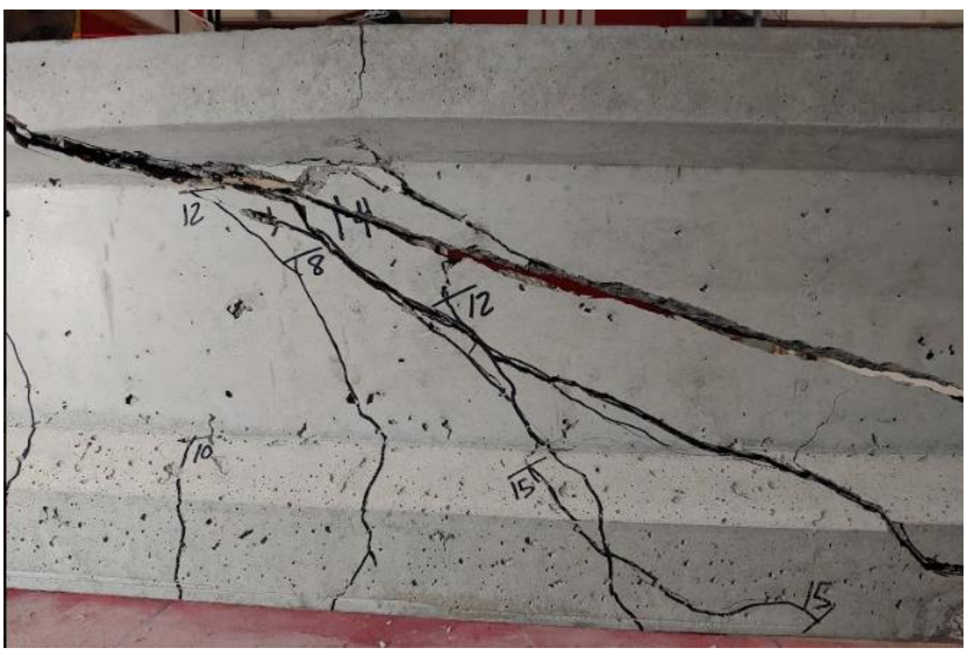

(b)

Figure 4-5: Ultimate failure crack in RC-B1 (a) and RC-B2 (b)

After the beams were unloaded, each beam was taken out of the testing frame for better visual analysis. The full unloaded beams are shown in Figure 4-6.

(a)

(b)

Figure 4-6: Unloaded beam RC-B1 (a) and RC-B2 (b)

4.3 Ultra-high-performance Concrete

A graphical representation of the data from the tests performed are presented in the following figures. Figure 4-7 shows the compressive strengths of the UHPC used in the beam specimens. Figure 4-8 shows a load-deflection plot for the three beam specimens. For UHPC-B3, the wire pots were removed during testing because the beam was almost resting on the wire pots after deflecting nearly 3 in. The first beam tested was loaded at 2 kip increments up until failure, whereas the last two beams were loaded at 5 kip increments until reaching 60 kips. This was due to the uncertainty of how the UHPC beams would fail. The periodic decreases in load coincided with pauses in the test to mark the cracks in the beams and take photographs. Together these graphs can provide insight into how the specimens responded to the loading.

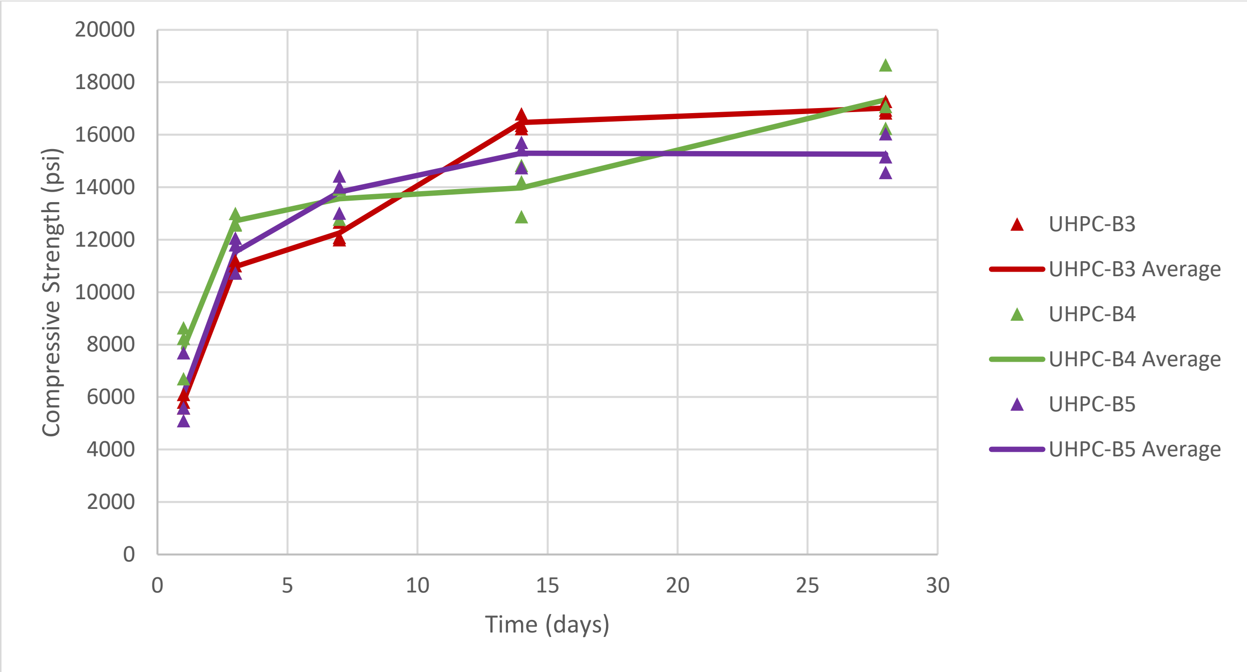

Figure 4-7 : Compressive strength of UHPC

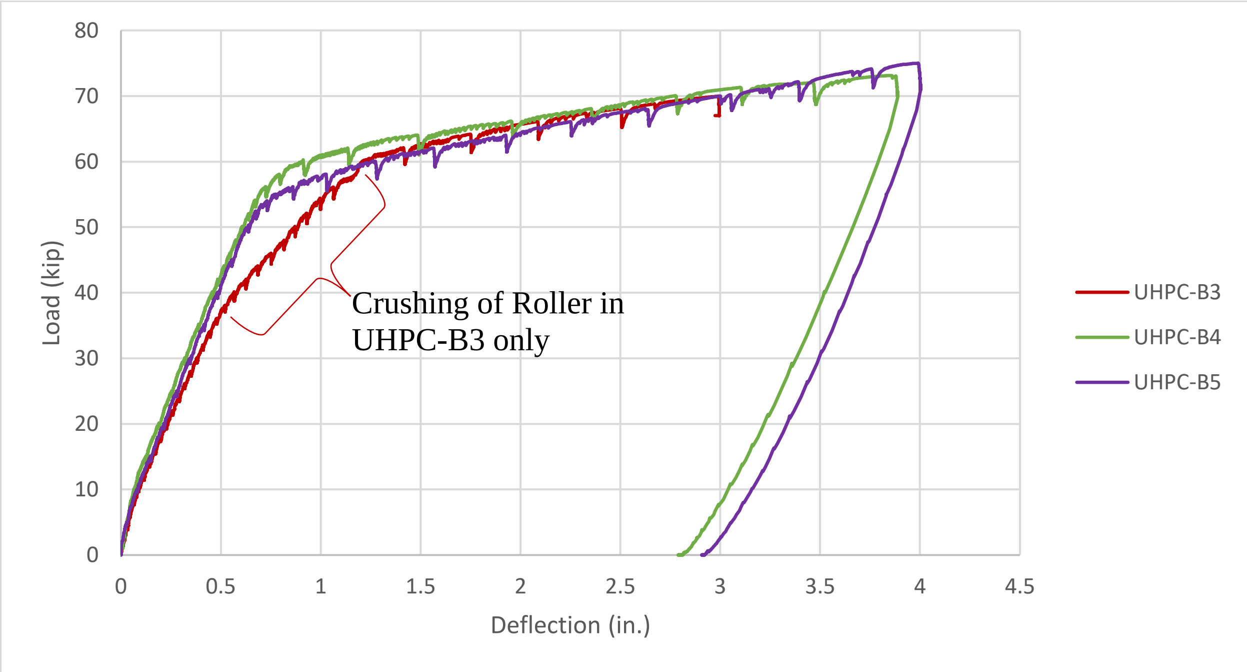

Figure 4-8: Load vs deflection for UHPC beams

In Figure 4-7, the compressive strength for UHPC-B5 appears to be lower at 28 days than the strength recorded on 14-day testing. The compressive strength for UHPC-B5 at 28 days is inconsistent with the expected strength based on the results from 1-, 3-, 7-, and 14-day tests. Based on this curve, it appears the UHPC-B5 mix ceased to gain strength after 14 days whereas concrete typically gains strength until fully cured at 28 days. The other two UHPC mixes displayed increasing strengths up to 28 days, indicating the mix does not develop more quickly than expected. Cylinders from the UHPC-B5 mix were tested at 35 days. The compressive strengths for these three specimens were: 18,627, 18,036, and 18,860 psi. This results in an average compressive strength of 18,510 psi. Because the compressive strength at 35 days was much higher than the results of 28-day testing, it would be illogical to assume that the strength gain ceased after 14 days. A linear interpolation of the 14-day and 35-day compressive strengths would likely be a better representation of the strength of UHPC-B5 at 28 days. Interpolating between 15,300 psi at 14 days and 18,510 psi at 35 days results in a strength of 17,420 psi for UHPC-B5 at 28 days.

The data in Figure 4-8 is strongly bi-linear. The only exception to this is the small section of the deflection curve for UHPC-B3 that diverges from the plots of the other two, indicated by the bracket. During testing, one of the steel support rollers crushed. This caused an increase in deflection that was not associated with the concrete but appears in the graph as a loss in stiffness for the concrete. A photograph of the roller under the beam is shown in Figure 4-9. Due to the crushing of the roller, the testing had to be stopped and restarted after replacing the support with a different steel roller. When the beam was fully unloaded, the laser level indicated a deflection of 0.5 in. which roughly matches the deflection of the described region, indicating that the deflection on the graph was primarily due to the roller crushing. The first test reached a load of nearly 60 kips, which resulted in significant cracking in the beam. When the beam was reloaded, it deflected more at lower loads, because of the decreased stiffness associated with cracking. During the second loading of UHPC-B3, the deflection exceeded 3 in. at which point the center of the beam was nearly resting on the wire pots. Due to these complications, the data presented for UHPC-B3 is from both tests spliced at 60 kips and cut off after the wire pots were removed, although the test was continued. Without the complications in the test, it is likely that the results for UHPC-B3 would have closely followed the results for the other beams.

Figure 4-9: Crushed roller under UHPC-B3

A summary of the results of the UHPC specimens is presented in Table 4-2. All beams were tested 28 days after casting. The deflection for the first beam was not measured in full due to removing the wire pots, but a deflection of 3.50 in. was recorded with the laser level attached to the spreader bar at the maximum load of the second test. This deflection is an underrepresentation of the true value because the beam was curved between the loading points, where the spreader beam remained straight. The compressive strength recorded in Table 4-2 for UHPC-B5 is the result of the three cylinders tested on day 28, but as described above, the strength was likely higher.

Table 4-2: Max results from UHPC specimens

	UHPC-B3	UHPC-B4	UHPC-B5
28-day f'c (psi)	17,020	17,340	15,260*
Load at Shear Failure	N/A	N/A	N/A
Max Load (kip)	72.96	73.12	75.00
Max Deflection (in.)	3.50	3.88	4.00

* The strength presented is from the 28-day compressive testing, linear interpolation suggests a strength of 17,420 psi

Flexural cracks began to appear first in all three UHPC beams. Because the loading increments changed after the first test, the markings on the second and third beam indicate a higher load for the initial cracks than UHPC-B3. The later beams were inspected at larger intervals making the load marked on the initial cracks less precise than the first UHPC beam. The middle section of the beams, where the flexural cracking occurred, are shown in Figure 4-10. The load coinciding with each photograph differs. Photographs after the beams were unloaded were used for comparison of the cracking.

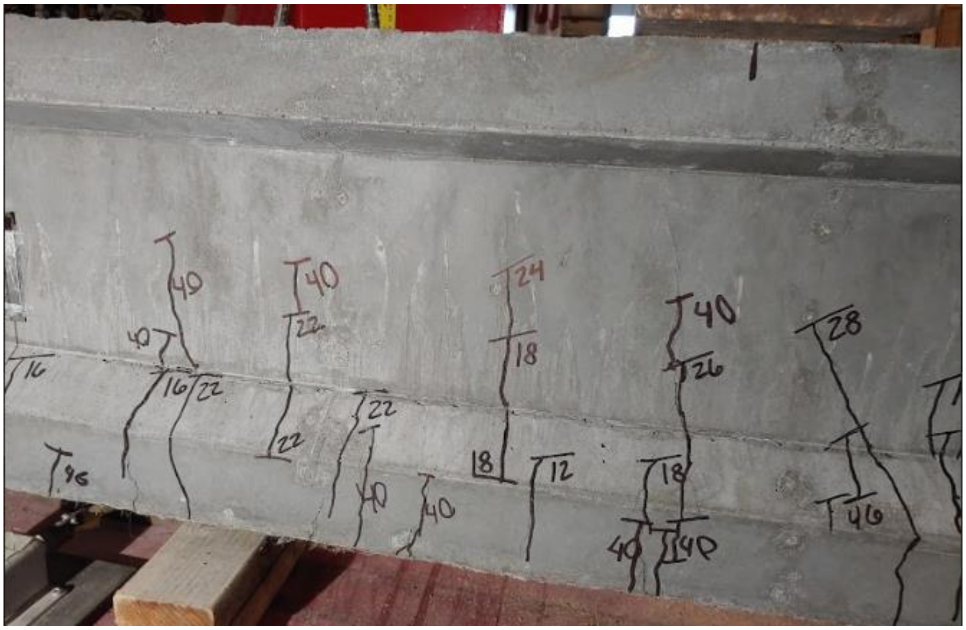

(a)

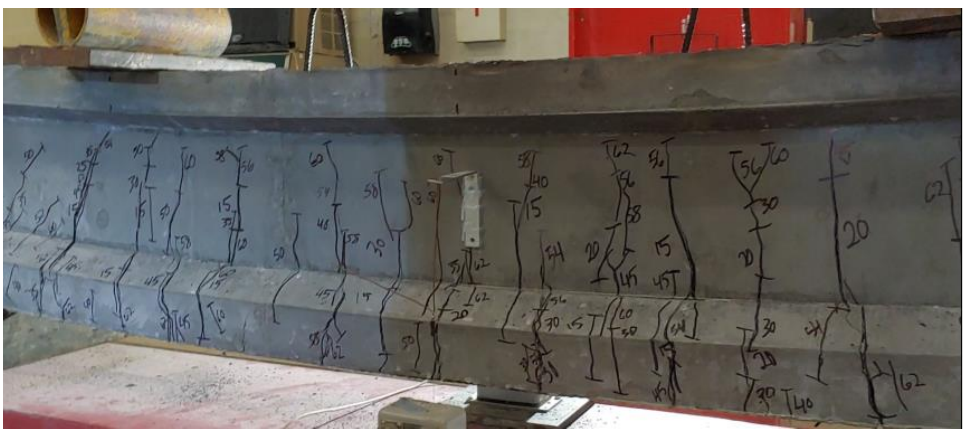

(b)

(c)

Figure 4-10: Flexural cracking of UHPC-B3 (a), UHPC-B4 (b), and UHPC-B5 (c)

The beams began to exhibit shear cracking after exceeding 30 kips. These cracks primarily appeared in the web and did not progress into either flange. These cracks did not widen significantly, but small parallel cracks did form as the loading progressed. The cracks are shown in Figure 4-11. UHPC-B3 was under 40 kips total load at the time of the photograph, while UHPC-B4 and UHPC-B5 were unloaded when each photograph was taken.

(a)

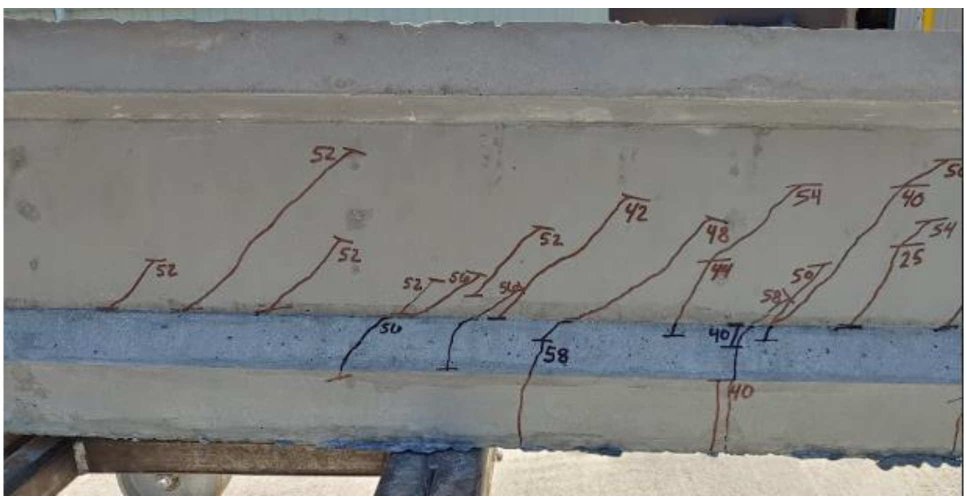

(b)

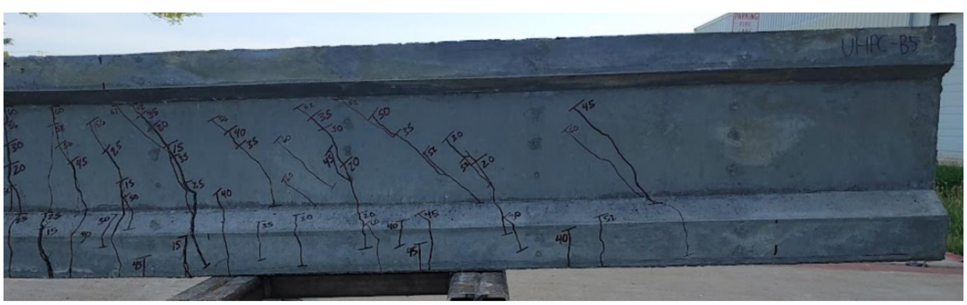

(c)

Figure 4-11: Shear cracking of UHPC-B3 (a), UHPC-B4 (b), and UHPC-B5 (c)

As the tests continued, the flexural cracks began to widen and the beams continued to deflect. The number of cracks that appeared also increased far beyond that of the Class AA beams. The number of cracks can be attributed to the higher load, but also was likely due to the presence of the steel fibers. More cracks formed as opposed to the already present cracks widening. This behavior is similar to how shear cracks propagate when crossing a stirrup, the steel keeps the crack from widening and allows for friction to still contribute to the stress transfer. UHPC-B3 buckled in the top flange at 73 kips. The tests for UHPC-B4 and UHPC-B5 were stopped before buckling occurred, however signs of the concrete crushing were present in the top flange. Figure 4-12 shows each beam as it approached the maximum load achieved.

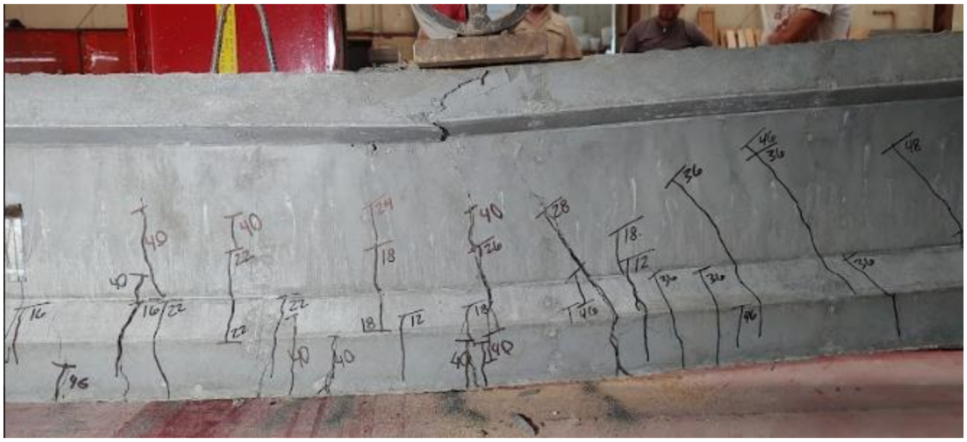

(a)

(b)

(c)

Figure 4-12: UHPC-B3 (a), UHPC-B4 (b), and UHPC-B5 (c) under load

As with the Class AA beams, the measurements from the load cell and wire pots were not stopped until the beams were fully unloaded. The beams were then removed from the testing frame. The large plastic deformations in the beams are shown in Figure 4-13, which can be quantified by the end of the curve in Figure 4-8. For UHPC-B3, the final deflection on the laser level was 2.25 in., indicating a recovery of 1.25 in. of deflection. This appears to be in line with the results from the other two UHPC beams, although the actual deflection measured is an underrepresentation as discussed earlier.

(a)

(b)

(c)

Figure 4-13: Unloaded UHPC-B3 (a), UHPC-B4 (b), and UHPC-B5 (c)

More photographs of the beams during and after testing can be found in the appendix.

5 Analysis

5.1 Introduction

This chapter will present the analysis of the results from the beam tests performed for this study. The results were compared to the appropriate ACI 318-19 (2019) equation for shear in beams. The results for the beam tests were also compared to a database of shear tests (Ortega, 2012). The beam cross section was designed to allow for shear failure with the UHPC. The Class AA concrete specimens were used as a control for the experiment.

5.2 Comparison to ACI Code and Shear Test Database

Equation 5-1 provides the expected shear capacity of concrete for sections with less than the minimum shear reinforcement. This equation comes from ACI 318-19 Table 22.5.5.1 (2019) and was used due to the exclusion of shear reinforcement in the section under shear stress. Embedded in this equation is a size factor, due to the non-linear relationship between depth and shear capacity. This factor can be calculated using Eq. 5-2, which is from ACI 318-19 Section 22.5.5.1.3 (2019). Variables are defined in the notation section of this paper. No axial load was applied to the beams during testing.

$$V_c = \left[8\lambda_s \lambda (p_w)^{1/3}\sqrt{f'_c} + \frac{N_u}{6A_g}\right] b_w d \qquad \text{(Eq. 5-1)}$$

$$\lambda_s = \sqrt{\frac{2}{1+\frac{d}{10}}} \leq 1 \qquad \text{(Eq. 5-2)}$$

The comparison of the shear force at failure from the test to the calculated capacity is presented in Table 5-1. The shear in the beam was calculated by dividing the value from the load cell in half due to the presence of the spreader beam. A ratio of 1.0 indicates an accurate prediction of the shear capacity. The ratio for both Class AA concrete specimens is close to 1.0.

Values larger than 1.0 indicate the equation is under-valuing the shear capacity. For the UHPC, the ratios average to 3.85, indicating the ACI Code (2019) does not predict the capacity of this concrete very closely. Also, none of the UHPC beams failed in shear, so the load from the test is at least the minimum for the shear capacity. In the ACI Code (2019), there is also a limit of 100 psi on the $\sqrt{f'_c}$ due to inexperience with concrete of higher strengths. This limit was not applied for analysis, which would have increased the ratios further. It should also be noted that the ratio of the tested shear capacity to the calculated capacity for UHPC-B5 would be 3.81 if the compressive strength was at 17,420 psi, as was suggest earlier.

Table 5-1: Results of test and shear equation

	V_{test} (kips)	ACI Capacity (kips)	Ratio
RC-B1	7.75	7.31	1.06
RC-B2	7.45	7.63	0.98
UHPC-B3	36.48	9.71	3.76
UHPC-B4	36.56	9.80	3.73
UHPC-B5	37.50	9.20	4.08

The calculated flexural capacity was approximately three times the anticipated shear capacity of the UHPC, and beyond that for the Class AA concrete. Based on the longitudinal reinforcement, the calculated flexural capacity for the beams was approximately 44 kips. The UHPC beams exceeded the anticipated shear capacity by 273% and the flexural by approximately 64%. The flexural capacity was calculated using strain compatibility and did not include the benefit of adding the steel fibers, which would explain the under prediction of the failure load. The simplified version of the shear equation uses $2\sqrt{f'_c}b_w d$. Based on the results from these tests, the factor could be replaced with a value of 9 and still be conservative. Ultimately, the UHPC beams tested did not fail in shear, meaning that the shear capacity is at least $9\sqrt{f'_c}b_wd$ for this mix, using 2% fibers. Figure 5-1 shows the same data as the plot of the load vs deflection curves. In this graph, the load was converted to the shear in the beam, and the shear was divided by $\sqrt{f'_c}b_wd$ to show just the coefficient needed to calculate the shear capacity.

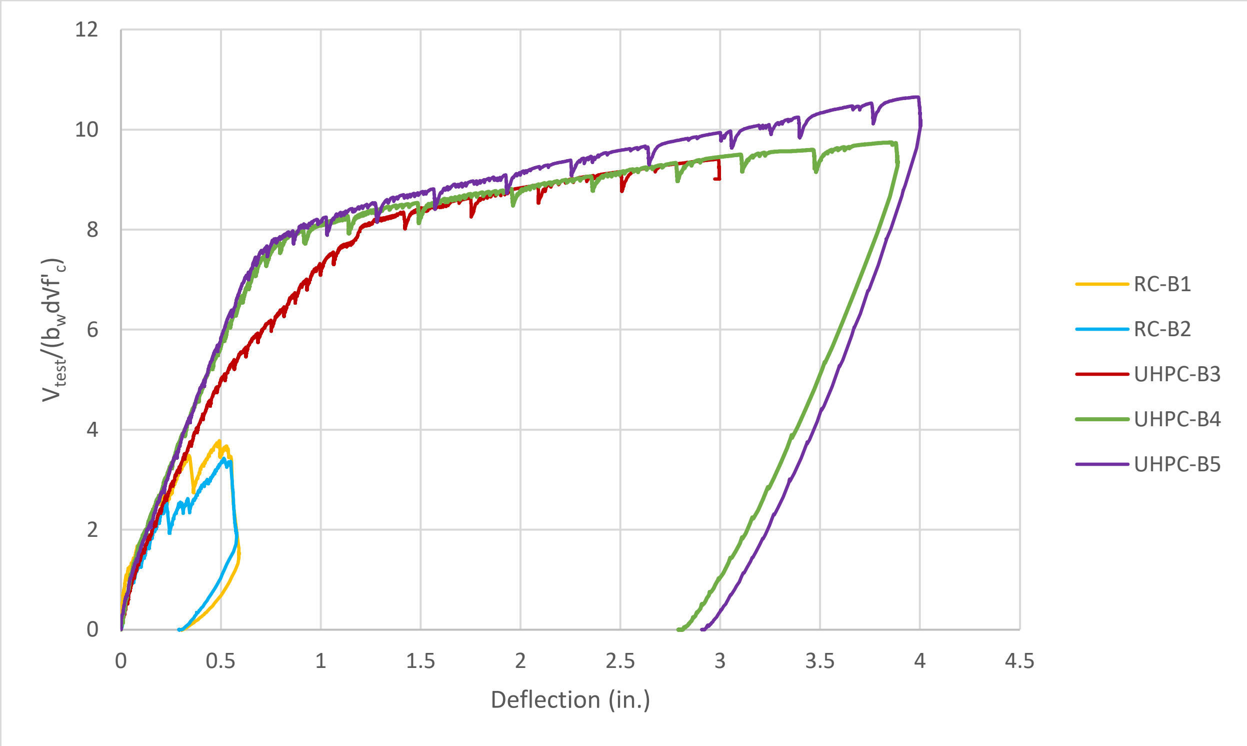

Figure 5-1: Leading coefficient for shear equation vs deflection

The same drop in load, that corresponded to a break, is present in the graph as before. This allows for these cracks to be shown as the corresponding coefficient. The graph also shows that the UHPC did not have a sudden drop in load at any point that would indicate a failure of the beam.

The beam deflection data is presented a second time, but with the linearly interpolated compressive strength for UHPC-B5, in Figure 5-2. This data is presented to show how closely grouped all three of the UHPC beams were in terms of the initial stiffness and beyond the yielding point.

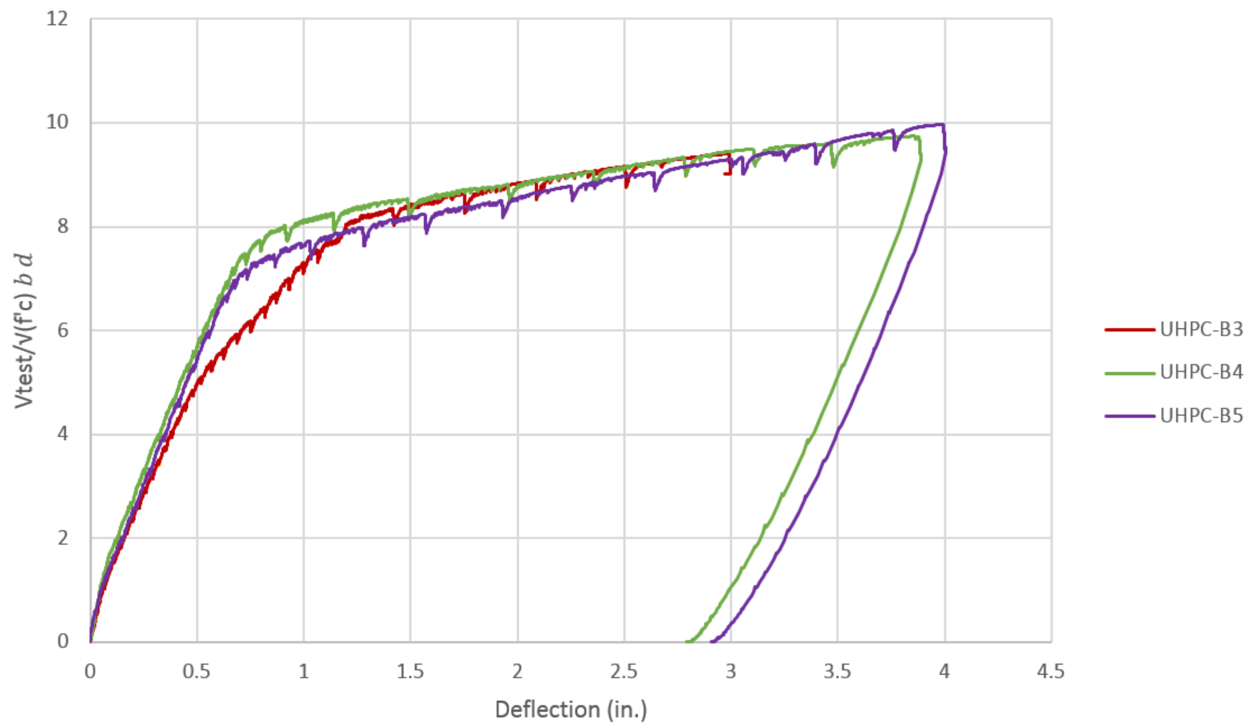

Figure 5-2: Shear load in UHPC normalized by shear equation, using the interpolated f'c

Figure 5-3 shows the shear failure loads versus the shear span-to-depth ratios for numerous previous studies (Ortega, 2012). The loads have been normalized the same way as above. The load at shear failure was plotted for the Class AA concrete beams from the current study. The maximum load achieved by the UHPC specimens was used for the plot, however, because the beams never reached a shear failure.

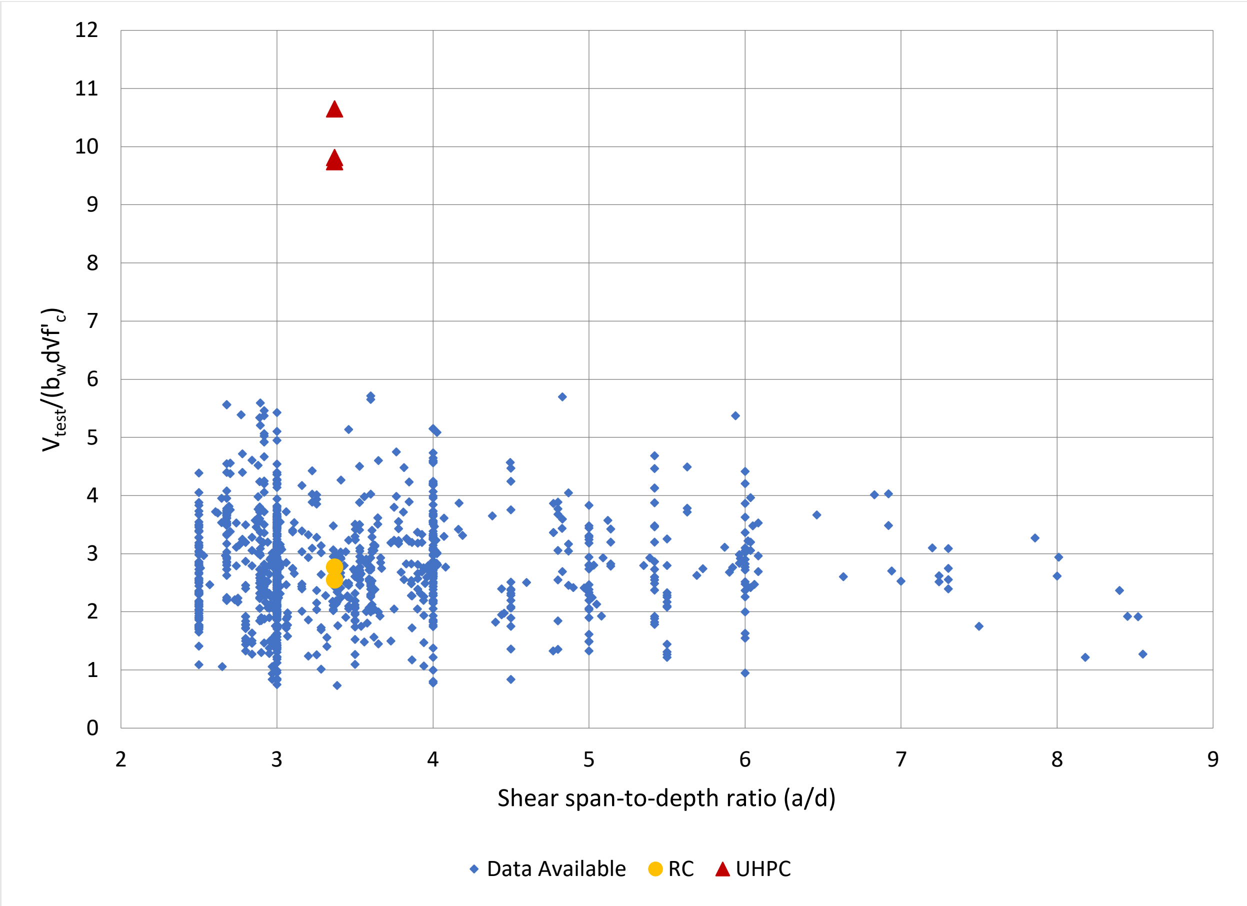

Figure 5-3: Tested shear capacity vs span-to-depth ratio

For these tests, the only variable that changes in the shear equation is the compressive strength of the concrete. Figure 5-3 shows that the control specimens fell comfortably within the middle of the available data. When plotted with the shear database, the results for the UHPC beams were significantly higher than the results for the conventional concrete of the same size and shape, as well as the normalized beam sections from the significant number of previous shear tests. As with the deflection plot, Figure 5-2, if the compressive strength of UHPC-B5 is taken as 17,420 psi, the variation of the results for the three UHPC mixes decreases significantly.

Table 5-2 shows the loads taken as shear failure compared to the beam properties to show the factor that could be used in the shear equation. Again, none of the three UHPC beams failed in shear, so the results presented are related to the maximum load during testing.

Table 5-2: Results for shear factor using interpolated f'c

	V_{test} (kips)	$\sqrt{f'_c}$ (psi)	$V_{test}/(b_w d\sqrt{f'_c})$
RC-B1	7.75	9,640	2.77
RC-B2	7.45	10,510	2.55
UHPC-B3	36.48	17,020	9.81
UHPC-B4	36.56	17,340	9.74
UHPC-B5	37.50	17,420	9.97

5.3 Comparison to French Association of Civil Engineering (AFGC) Design Code

Design guidance for Ultra-high Performance Fiber-Reinforced Concrete (UHPFRC) was developed and published in 2016 in France. This code calculates the shear capacity in three parts, $V_{Rd,c}$, $V_{Rd,s}$, and $V_{Rd,f}$. These represent the contributions to the shear strength of the concrete, the stirrups, and the fibers, respectively. The equation for $V_{Rd,c}$ is similar to the ACI (2019) shear equation but would have a factor of 1.7, as opposed to a factor of 2. In both cases, the contribution from stirrups is 0, due to a lack of stirrups in the tested region. Lastly, the $V_{Rd,f}$ factor calculates the added shear strength from the steel fibers based on the area under shear, the post-cracking strength and the crack inclination. The post-cracking strength was not measured in this study, but the shear cracking in the UHPC did remain very thin, while the flexural cracks widened to beyond the 0.3 mm, the limit set for in service by the AFGC. For these shear design equations to be more accessible, more testing must be done to predefine the minimum post-cracking strength, which depends on the member depth, crack width, type of fibers used and distribution of fibers. The results from these equations would likely be quite conservative, but more accurate than the current ACI shear equation (2019).

5.4 Contributions of the UHPC Steel Fibers

The fibers used in the UHPC are straight copper coated steel fibers. According to ACI 318-19 Section 26.4.1.6.1 (2019), these fibers may not be considered to contribute shear resistance. To qualify as shear reinforcement, the ACI Code (2019) requires the use of hooked or crimped steel fibers. However, the steel fibers used in the UHPC provide a much higher tensile strength than typically assumed for concrete, which changes how the cracks develop. This property of the UHPC is the reserve tensile capacity, which is approximately 0.7 ksi (Looney, 2021). The progression of both the shear and flexural cracks for the UHPC differed from the conventional concrete significantly. In the UHPC, the cracks did not widen as they did in the Class AA beams. Instead, parallel cracking occurred in the UHPC, meaning a larger number of smaller cracks occurred. Also, according to the commentary within the ACI Code (2019), steel fibers can restrain the growth of inclined shear cracking, improving the ductility of the beam, which likely occurred even though the fibers were not hooked or crimped due to the better bonding ability of UHPC.

6 Findings, Conclusions, and Recommendations

6.1 Introduction

This final chapter will present the conclusions drawn from this research, as well as recommendations for future research. The objective of this study was to evaluate the shear performance of UHPC. Large scale beams were tested under third point loading to discover the shear capacity of UHPC.

6.2 Findings

The findings of the study performed are presented below:

- The Class AA mixes achieved strengths of 9,640 and 10,510 psi.
- Both Class AA beams failed in shear.
- The total load at shear failure for the Class AA beams was 15.50 and 14.89 kips, which resulted in a shear failure load of 7.75 and 7.45 kips, respectively.
- The maximum total loads achieved by the Class AA beams were 21.97 and 20.02 kips.
- At its maximum load, each Class AA beam abruptly buckled the top flange.
- The maximum deflections in the Class AA beams were 0.59 and 0.58 in.
- The UHPC mixes achieved strengths of 17,020, 17,340, and 15,260 psi (although the strength of the mix may have been closer to 17,420 psi).
- The UHPC beams did not fail in shear.
- The maximum total loads achieved by the UHPC beams were 72.96, 73.12, and 75.00 kips, which corresponds to a maximum shear load of 36.48, 36.56, and 37.50 kips, respectively.

- The maximum deflections achieved by the UHPC beams were 3.5 (approximately due to removing wire pot), 3.88, and 4.00 in.
- Only the first UHPC beam experienced an abrupt buckling in the top flange.
- All UHPC beams experienced crushing of the concrete in the top flange.

6.3 Conclusion

Based on the findings of this study, the following conclusions were drawn:

- The Class AA beams failed in shear near the predicted loads based on the ACI Code (2019), with capacities that averaged $2.61\sqrt{f'_c}b_w d$, compared to the standard shear design strength equation of $2\sqrt{f'_c}b_w d$.
- The ACI Code (2019) is an adequate predictor of shear in Class AA concretes.
- The UHPC beams had shear capacities of at least $9.81\sqrt{f'_c}b_w d$, $9.74\sqrt{f'_c}b_w d$, and $10.65\sqrt{f'_c}b_w d$, all well above the standard shear design strength equation of $2\sqrt{f'_c}b_w d$. The UHPC beams likely had even higher shear capacities but, unfortunately, failed due to crushing of the top flange.
- The ACI Code (2019) requires modification in order to accurately predict the shear strength in UHPC.
- The UHPC beams exceeded the expected shear capacity by at least 270%.
- The presence of fibers in UHPC beams significantly increased the shear capacity of the beams, likely due to the improved tensile strength.

6.4 Recommendations

More research would be necessary to validate the claims made in this thesis and verify the extent to which each is applicable. Based on the results of this study, the following recommendations are presented:

- Use the same mix, but test beams of similar size with wider top flanges and higher reinforcement ratio to prevent flexural failure.
- Test identical beams with a lower dosage of fibers to find correlation between fiber percentage and shear resistance.
- Examine anchorage of steel fibers in UHPC due to bonding, as opposed to mechanical, to qualify as shear resistance as with hooked or crimped steel fibers.
- Consider adjusting the factor in the shear equation from a value of 2 to a value of 9 for UHPC with steel fibers.
- Consider instead adding a factor to the shear equation that relates to the percentage of steel fibers, given more research is conducted to find a proper correlation.
- Examine new possibilities for shear capacity that relate directly to UHPC tensile capacity, to avoid needing the post-cracking strength.

References

ACI Committee 318, (2019). Building Code Requirements for Structural Concrete and Commentary (ACI 318-19). American Concrete Institute, Farmington Hills, MI.

Bahij, S, Adekunle, SK, Al-Osta, M, Ahmad, S, Al-Dulaijan, SU, Rahman, MK. Numerical investigation of the shear behavior of reinforced ultra-high-performance concrete beams. Structural Concrete. 2018; 19: 305– 317. <https://doi-org.ezproxy.lib.ou.edu/10.1002/suco.201700062> (accessed March 10, 2022)

Campos, R. 2021. "Effect of Fiber Content on Tensile Strength of Non-Proprietary Ultra High Performance Concrete." M.S. Thesis, The University of Oklahoma, Norman, OK. < https://shareok.org/handle/11244/326674?show=full> (accessed May 13, 2022)

Cuenca, Estefanía, Pedro Serna Ros, and María José Pelufo Carbonell. "Structural behavior of self-compacting and fiber reinforced concrete under shear loading." *Symposium of the International Association for Shell and Spatial Structures (50th. 2009. Valencia). Evolution and Trends in Design, Analysis and Construction of Shell and Spatial Structures: Proceedings*. Editorial Universitat Politècnica de València, 2009.

de Montaignac, R., Massicotte, B., Charron, JP. Design of SFRC structural elements: post-cracking tensile strength measurement. *Material Structures* 45, 609–622 (2012). <https://doi.org/10.1617/s11527-011-9784-z> (accessed July 23, 2022)

Drury, Jonathan. Shear Performance of Non-Traditional Concrete (2018). OU – Dissertations, ShareOK.org. < https://shareok.org/handle/11244/301339> (accessed May 1, 2022)

Floyd, Royce W., Volz, Jeffery S., Looney, Trevor, Mesigh, Michael, Ahmadi, Mujtaba, Roswurm, Stephen, Huynh, Phuoc, Manwarren, Michelle. "Evaluation of Ultra-High-Performance Concrete, Fiber Reinforced Self-Consolidating Concrete, and MALP Concrete for Prestressed Girder Repair (FHWA-OK-21-03)." *ShareOK*, University of Oklahoma, 1 Feb. 2021, <https://shareok.org/handle/11244/330981. > (accessed March 7, 2022)

Graybeal, Benjamin A., Baby, Florent. "Tension Testing of Ultra-High Performance Concrete (FHWA-HRT-17-053)." Federal Highway Administration, U.S. Department of Transportation, Feb. 2019, <FHWA-HRT-17-053: Tension Testing of Ultra-High Performance Concrete (dot.gov)> (accessed July 24, 2022)

John, Emerson E., Edmundo D. Ruiz, Royce W. Floyd, and W. Micah Hale. "Transfer and Development Lengths and Prestress Losses in Ultra-High-Performance Concrete Beams." Transportation Research Record 2251, no. 1 (January 2011): 76–81. < https://doi.org/10.3141/2251-08. >, (accessed March 7, 2022)

Lepissier, K.J.G. 2020. "Tensile Behavior of Ultra-High Performance Concrete Under Direct Tension." M.S. Thesis, The University of Oklahoma, Norman, OK. < https://shareok.org/handle/11244/325362> (accessed May 13, 2022)

Looney, Trevor. (2021). "Development of a novel apparatus to determine the multiaxial tensile failure criteria for ultra-high performance concretes." Ph.D. Dissertation, The University of Oklahoma, Norman, OK. <https://shareok.org/handle/11244/331088> (accessed June 18, 2022)

Ortega, C.A. (2012). “Shear and Fracture Behavior of High-Volume Fly Ash Reinforced Concrete for Sustainable Construction,” Ph.D. Dissertation, Missouri University of Science and Technology, Rolla, MO.

Pourbaba, M., Joghataie, A., & Mirmiran, A. (2018). Shear behavior of ultra-high-performance concrete. Construction and Building Materials, 183, 554–564. <https://doi.org/10.1016/J.CONBUILDMAT.2018.06.117 > (accessed February 12, 2022)

Reineck, Karl – Heinz, Kuchma, Daniel A., Fitik, Birol, "Research Report: Extended Databases with Shear Tests on Structural Concrete Beams without and with Stirrups for the Assessment of Shear Design Procedures," United States of America Nuclear Regulating Commission, 2012 < https://www.nrc.gov/docs/ML1926/ML19262F141.pdf>, (accessed March 10, 2022)

Solutions, UHPC. “Quick Guide to the History of UHPC.” Quick Guide to the History of UHPC, UHPC Solutions, 2019,< https://www.uhpcsolutions.com/blog/quick-guide-to-the-history-of-uhpc#:~:text=UHPC%20was%20officially%20coined%20in,in%20applications%20in%20North%20America.&text=The%20U.S.%20Army%20Corps%20of,a%20bridge%20in%20Quebec%2C%20Canada.> (accessed March 10, 2022)

Vance, Clark. “Mars Hill Bridge.” *Bridgehunter.com*, 12 Sept. 2012, <https://bridgehunter.com/ia/wapello/mars-hill/> (accessed April 26, 2022)

Voo, Yen Lei, Wai Keat Poon, and Stephen J Foster. "Shear Strength of Steel Fiber-Reinforced Ultrahigh- Performance Concrete Beams without Stirrups." Journal of Structural Engineering (New York, N.Y.) 136, no. 11 (2010): 1393-400.

Voytko, Danielle, Calvi, Paola M., Stanton, John. “Shear strength of ultra high-performance concrete.” Engineering Structures Volume 255, (2022). University of Washington. <https://doi.org/10.1016/j.engstruct.2022.113961.> (accessed July 23, 2022)

Wallace, Kodi. (2016). Performance of Fiber-Reinforced Eco-Friendly Concrete for Bridge Structures. M.S. Thesis, The University of Oklahoma, Norman, OK. < https://shareok.org/handle/11244/44899> (accessed October 3, 2021)

Appendix

Figure A-1: Broken Class AA cylinder type 4

Figure A-2: Broken Class AA cylinder type 1

Figure A-3: Broken Class AA cylinder type 2

Figure A-4: UHPC cylinders after grinding

Figure A-5: Broken UHPC cylinder type 2

Figure A-6: Broken UHPC cylinder type 3

Figure A-7: RC-B1 in testing frame

Figure A-8: End of RC-B1 in testing frame

Figure A-9: Center of RC-B1 in testing frame

Figure A-10: Wire pot attached to beam

Figure A-11: Shear cracking in RC-B1 SW side

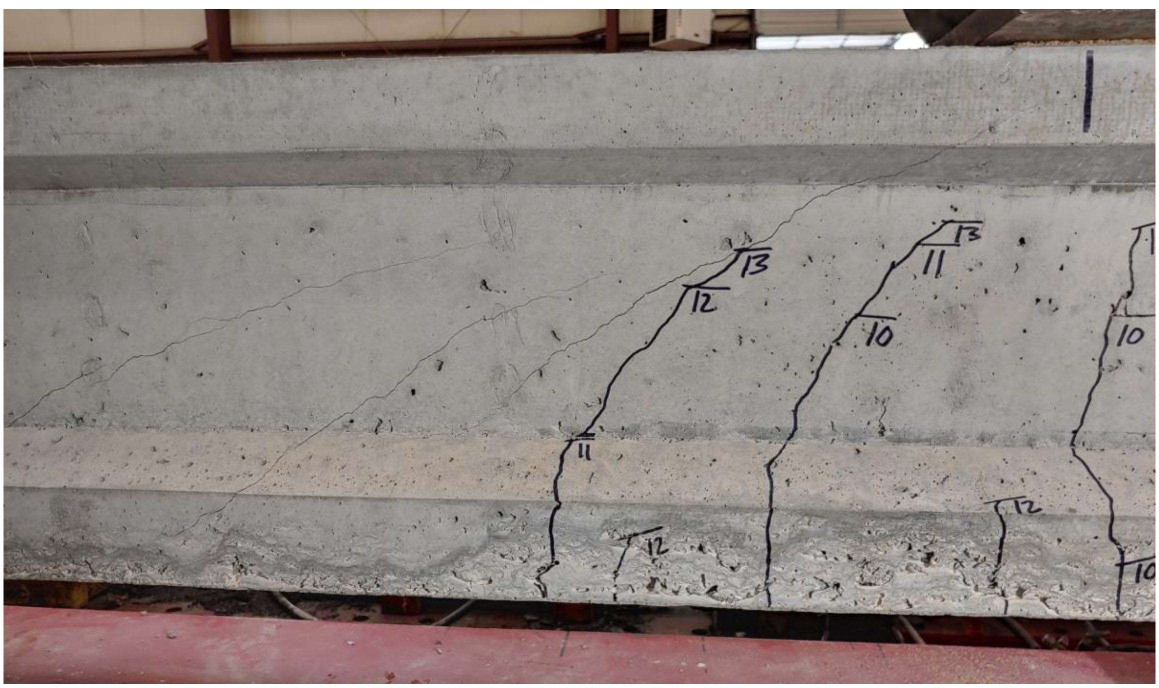

Figure A-12: Shear cracking in RC-B1 SE side

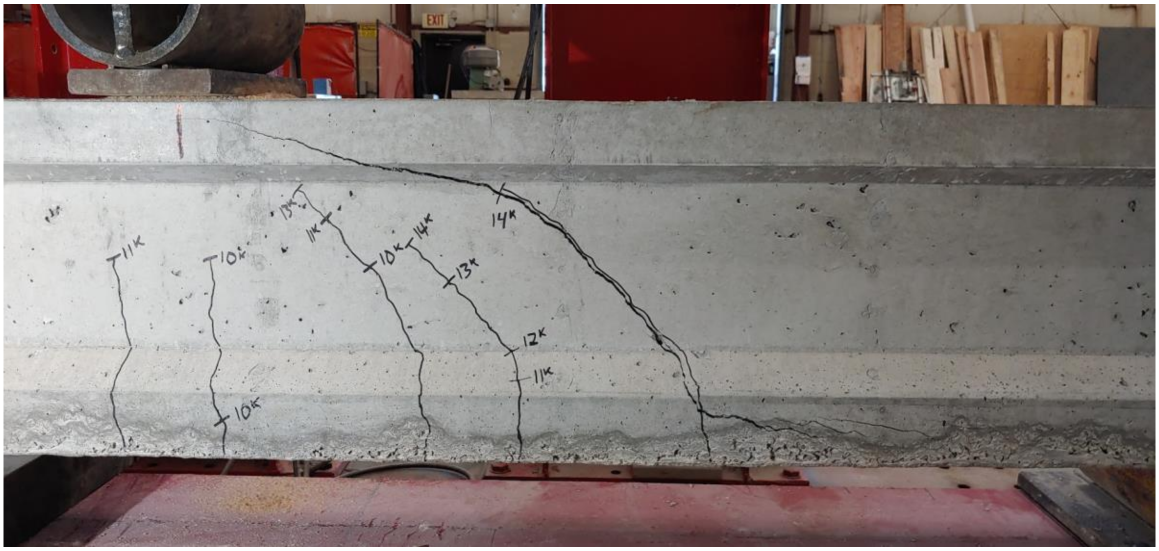

Figure A-13: Shear cracking in RC-B1 NE side

Figure A-14: Shear cracking in RC-B1 NE side after buckling

Figure A-15: Shear cracking in RC-B1 NW side after buckling

Figure A-16: Flexural cracking in RC-B1 W side near max load

Figure A-17: Flexural cracking in RC-B1 E side after buckling

Figure A-18: Shear crack revealing crosstie

Figure A-19: Buckling of top flange in RC-B1 top view

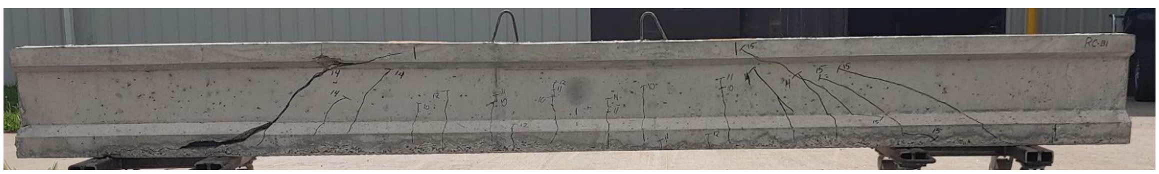

Figure A-20: Full view of RC-B1 W side

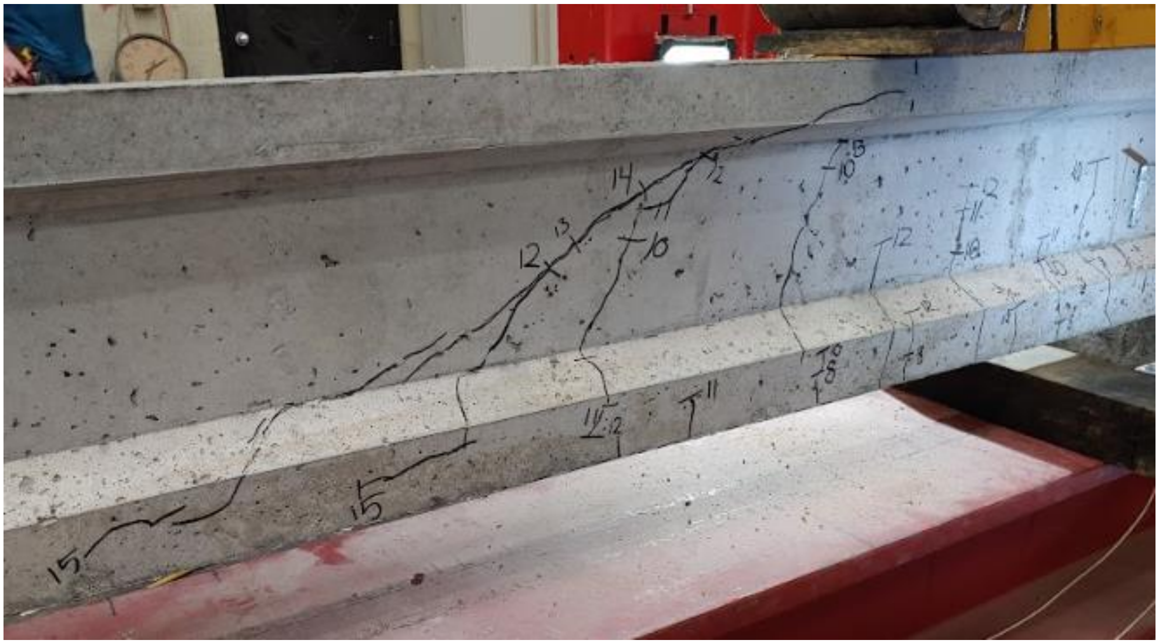

Figure A-21: Shear cracking in RC-B2 NW side

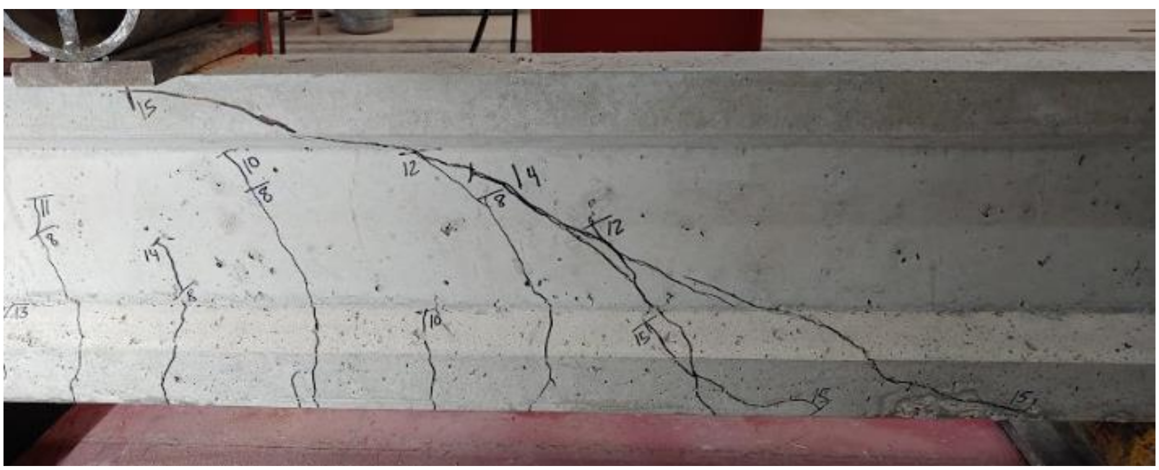

Figure A-22: Shear cracking in RC-B2 NE side

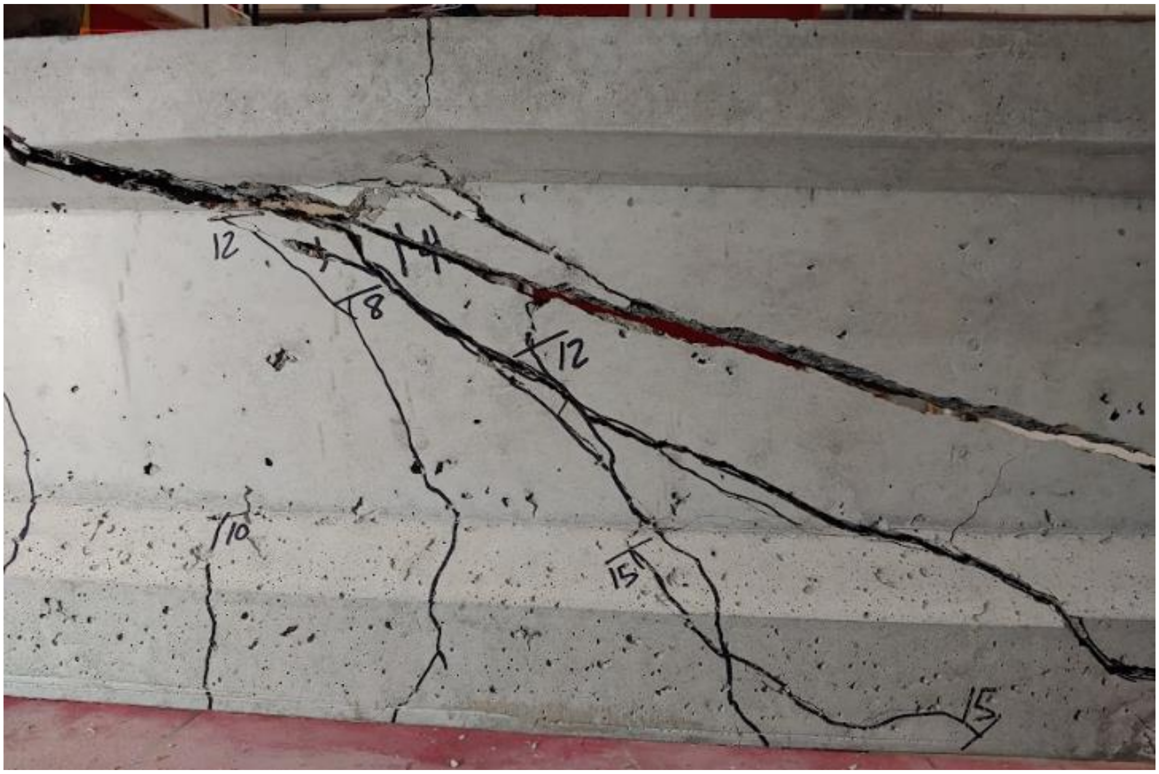

Figure A-23: Shear cracking in RC-B2 NE side after buckling

Figure A-24: Shear cracking in RC-B2 NW side after buckling

Figure A-25: Flexural cracking in RC-B2 E side

Figure A-26: Flexural cracking in RC-B2 W side

Figure A-27: Buckling of top flange in RC-B2 top view

Figure A-28: Full view of RC-B2 W side

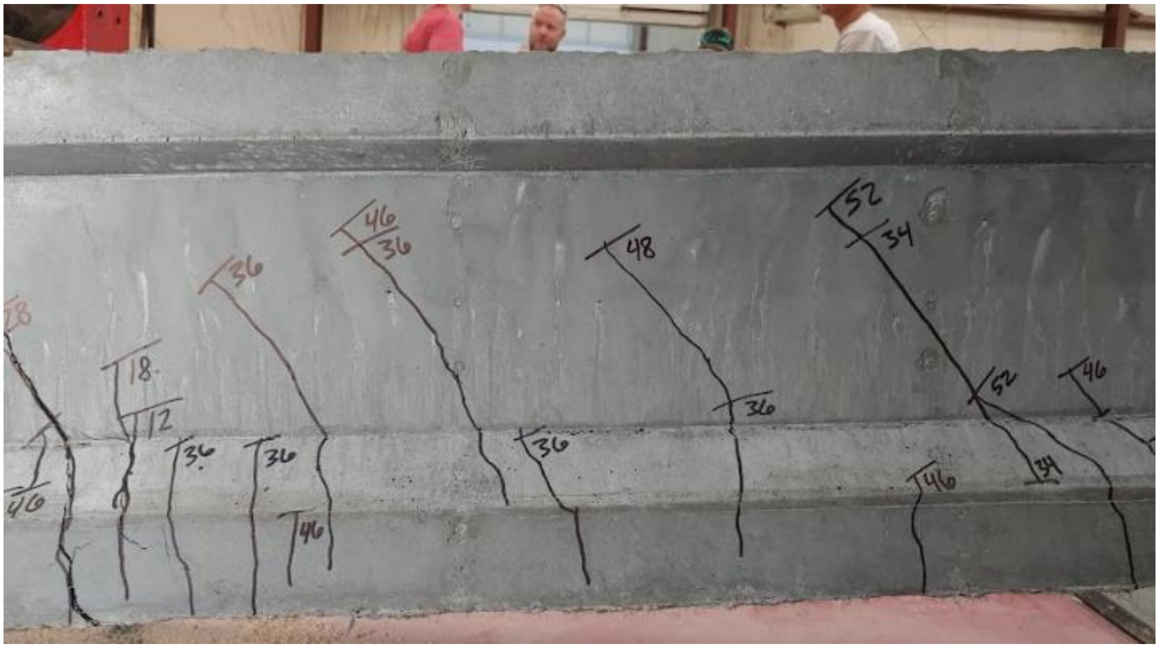

Figure A-29: Shear cracking in UHPC-B3 NE side

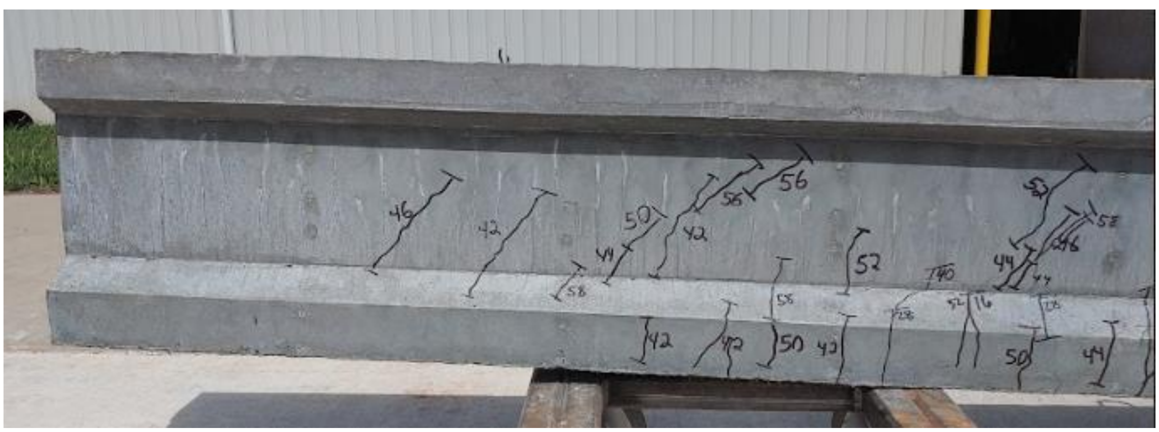

Figure A-30: Shear cracking in UHPC-B3 NW side

Figure A-31: Flexural cracking in UHPC-B3 E side

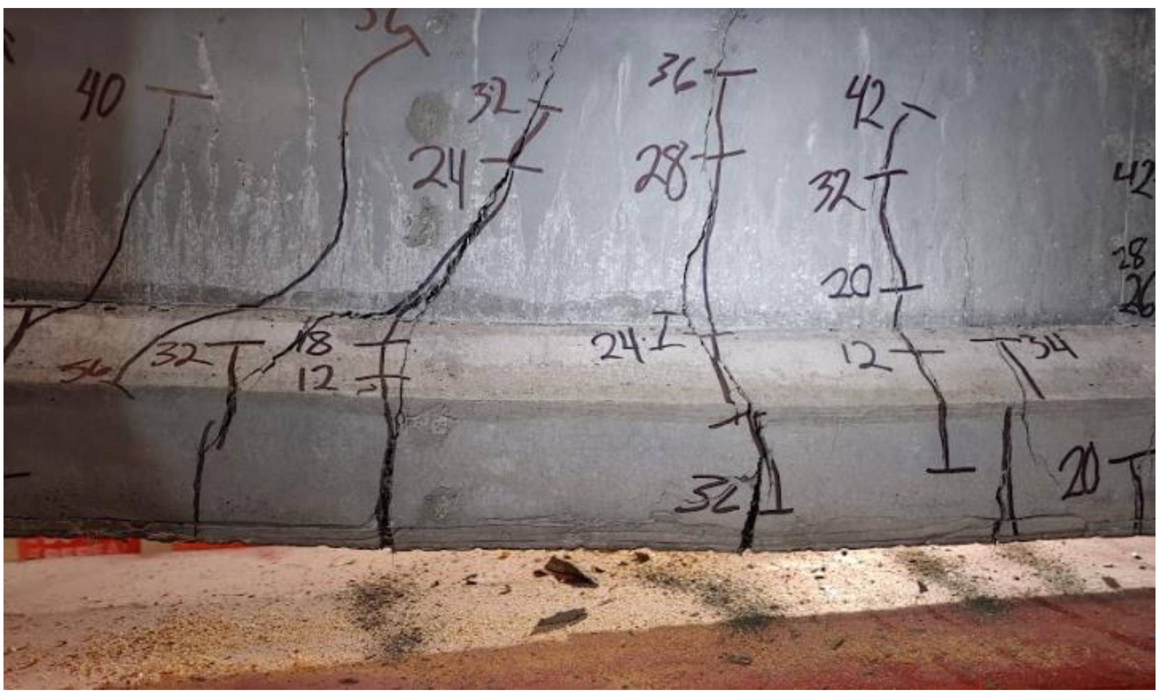

Figure A-32: Flexural cracking in UHPC-B3 W side

Figure A-33: Crushing of the concrete in UHPC-B3 NW side after buckling

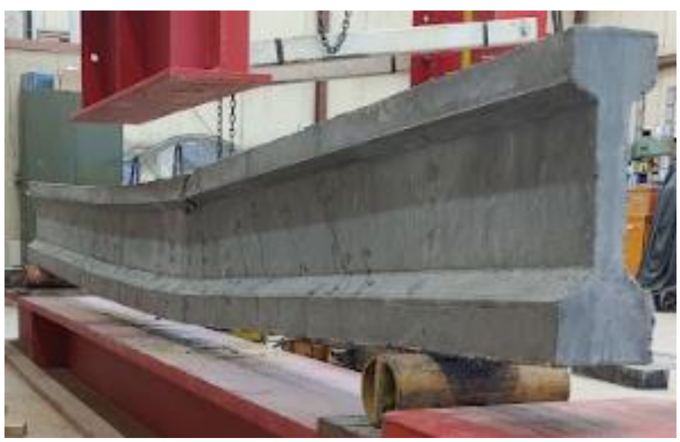

Figure A-34: Deflection of UHPC-B3

Figure A-35: Cracks across bottom of UHPC-B3

Figure A-36: Angled crack with steel fibers in UHPC-B3

Figure A-37: Full view of UHPC-B3 E side

Figure A-38: Top rollers on UHPC-B4 with wider bearing plates

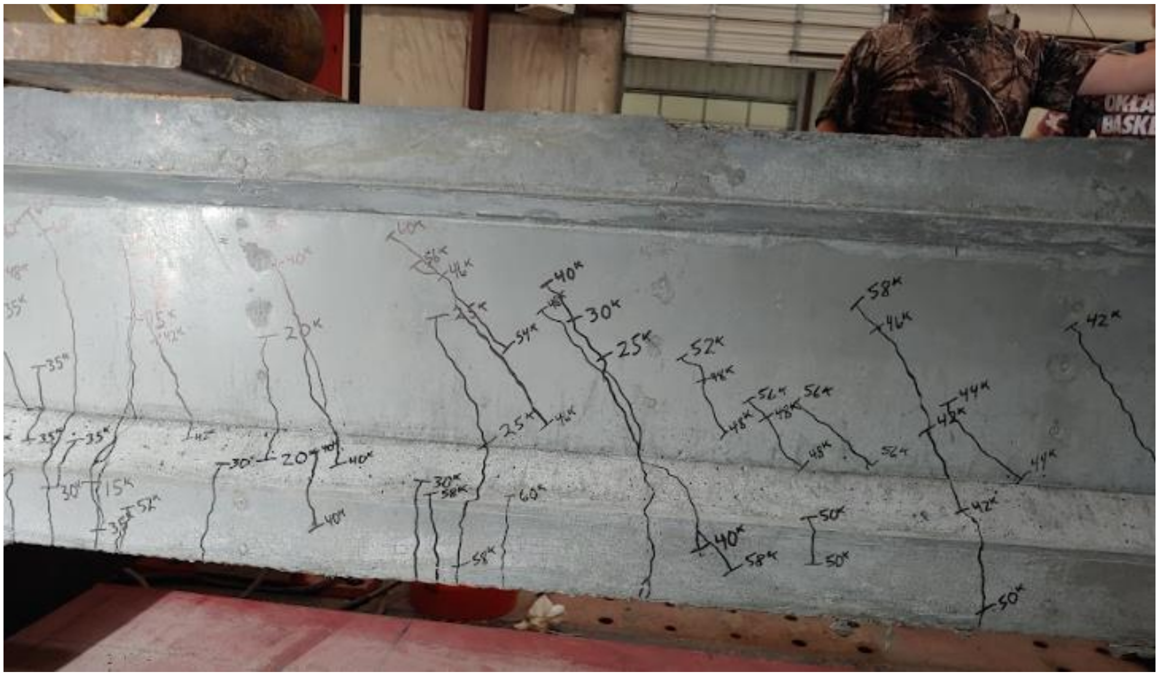

Figure A-39: Shear cracking in UHPC-B4 NE side

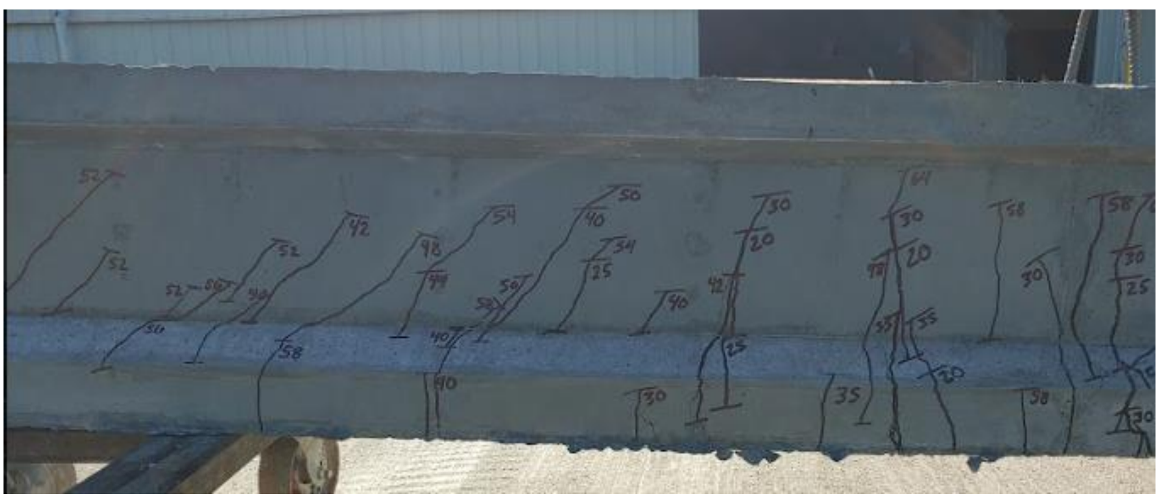

Figure A-40: Shear cracking in UHPC-B4 SE side

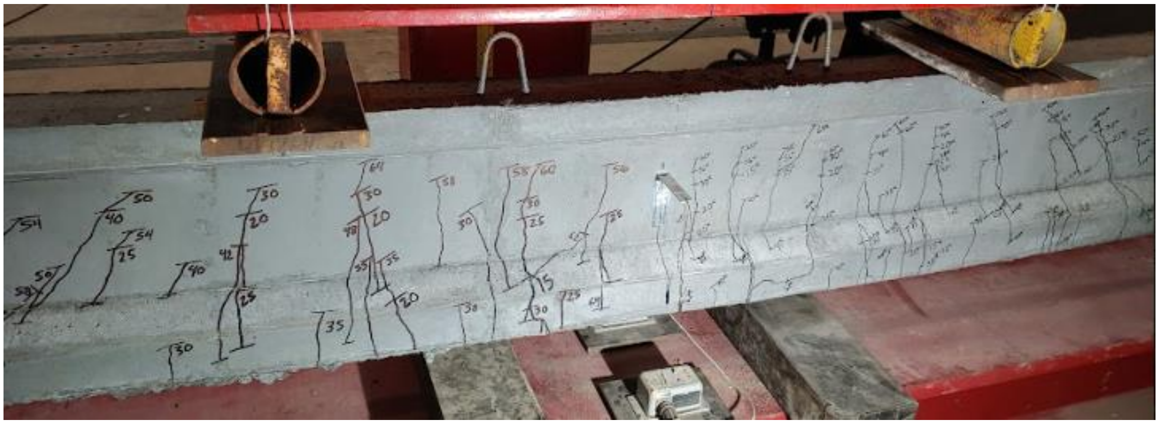

Figure A-41: Flexural cracking in UHPC-B4 E side

Figure A-42: Flexural cracking in UHPC-B4 W side

Figure A-43: Cracking in UHPC-B4 center of bottom flange W side

Figure A-44: Crushing of concrete between loading point in UHPC-B4 W side

Figure A-45: Deflection of UHPC-B4

Figure A-46: Cracking in UHPC-B5 NE side

Figure A-47: Cracking in UHPC-B5 SE side

Figure A-48: Cracking in UHPC-B5 NW side

Figure A-49: Cracking in UHPC-B5 SW side

Figure A-50: Crushing of concrete in UHPC-B5 in middle section

Figure A-51: Permanent deflection of UHPC-B5

Figure A-52: Comparison of deflection at ends of all beams